Particle Characterization for an Eight Inch Wafer Tungsten Chemical Vapor Deposition System

by

Troy Morrison

S.B. Materials Science and Engineering
Massachusetts Institute of Technology
(1993)

Submitted to the Department of Materials
Science and Engineering in Partial Fulfillment
of the Requirements for the Degree of

MASTER OF SCIENCE IN MATERIALS SCIENCE AND ENGINEERING

at the
Massachusetts Institute of Technology
February 1994

Signature of Author .....
Department of Materials Science and Engineering
January 14, 1994

Certified By .....
Lionel C. Kimerling
Professor of Materials Science and Engineering

Accepted By .....
Carl V. Thompson II
Professor of Electronic Materials
Chair, Department Committee on Graduate Students

Particle Characterization for an Eight Inch Wafer Tungsten Chemical Vapor Deposition System

by
Troy Morrison

Submitted to the Department of Materials
Science and Engineering in Partial Fulfillment
of the Requirements for the Degree of

MASTER OF SCIENCE IN MATERIALS SCIENCE AND ENGINEERING

at the
Massachusetts Institute of Technology
February 1994

ABSTRACT

Semiconductor manufacturing is an exciting field where people, equipment and technology have to be managed for fabrication of products. Even though a company may have a good product design and process, the real key to a competitive advantage and market share lies in a company's ability to manufacture the products in high volume at the lowest possible cost. Since the value of silicon wafers increases as they progress toward the backend of a process flow, overcoming yield problems associated with metallization can be a giant step in the direction towards lower costs and greater profits. Never before has this been more critical than with the growing implementation of multilevel interconnect technology and its associated multitude of repetitive steps. Because reducing defect-related yield losses can result in multiple reductions in the total defect density, particle characterization for each step in the backend process flow clearly becomes a high priority.

A new laser-based contamination analyzer is implemented to monitor optical defects on blanket tungsten films deposited by a tungsten Low Pressure Chemical Vapor Deposition (LPCVD) system. After establishing the new tool, median particle levels, control limits and trend data for the new blanket film particle analyzer are compared to the existing bare wafer contamination analyzer in order to identify an effective particle monitoring strategy.

By implementing a short loop integrated monitor, defects were tracked through different thin film layers in the metallization process. From this data the optical defects caused by tungsten deposition are determined and compared to other steps in the backend process flow. A strong positive correlation is observed between optical and electrical defect levels.

A technique is developed for the detection and characterization of light scattering defects on deposited tungsten films. Using atomic force microscopy (AFM), and optical and electrical probe tools, we characterize the surface roughness, reflectivity and resistivity of blanket tungsten films of various thicknesses and varying process parameters. A correlation is observed between film thickness and N_2 gas flow rates, and the surface roughness, reflectivity and resistivity. SEM/Energy Dispersive X-ray analysis of particles on the optimal tungsten film identified the composition of the particles. A laser-based contamination analyzer together with an optical microscope determined the particle size distribution. Hardware particle sources were then identified by matching the hardware chamber and reactant compositions to the elemental composition of the defect. The particle size distribution of distinct defect modes was also matched to hardware elements.

Thesis Advisor:

Lionel C. Kimerling, Professor of Materials Science and Engineering

Acknowledgments

Nearly a year of research, engineering and writing resulted in this document which could never have been accomplished without the assistance of numerous people.

I would like to thank my supervisor at Intel, Sanjay Tripathi, and my advisor at MIT, Lionel Kimerling, for their guidance, encouragement, inspiration and support. In addition I gratefully acknowledge the support and resources made available to me through Intel's D2 Technology and Manufacturing Center as well as the Materials Technology Group.

Many thanks to Premilla Patel for her particle elemental characterization as well as Leonard Kulig for his assistance in Atomic Force Microscopy. Without the invaluable tutoring from Rick Mayer on various tool skills ranging from contamination analyzers to optical review stations I could never have performed this work.

To Bonnie, Byron, Kingman, Helen, Chris and all the other Co-Ops who made working at Intel more fun and exciting. To Cindy Romero, who worked hard to get me my a position at Intel and worked even harder in guiding a highly successful college recruiting program.

Special thanks go to my parents, Barry and Joyce Morrison and my sister Tracy Morrison, for their concern and support over the years. My attendance at MIT would never have been possible had they not given me the opportunity to explore life outside of Wisconsin.

List Figures

List of Tables

Chapter One
Introduction

1.1 Project Motivation

Semiconductor manufacturing is an exciting field where people, equipment and technology have to be managed for fabrication of products. Even though a company may have a good product design and process, the real key to seeking a competitive advantage and market share lies in a company's ability to manufacture the products in high volume at the lowest possible cost. Since the value of silicon wafers increases as they progress toward the backend of a process flow, overcoming yield problems associated with metallization can be a giant step in the direction towards lower costs and greater profits. Never before has this been more critical than with the growing implementation of multilevel interconnect technology and its associated multitude of repetitive steps. Because reducing defect-related yield losses can result in multiple reductions in the total defect density, particle characterization for each step in the backend process flow clearly becomes a high priority.

1.2 Project Objectives

With the advent of multilevel interconnect technology, Low Pressure Chemically Vapor Deposited (LPCVD) tungsten has become widely used in device fabrication for vias and contacts due to its excellent step coverage, high resistance to electromigration and low resistivity. With sub-micron device geometries, there is an increasingly greater emphasis on detecting, containing and eliminating defects on deposited films. The first objective of this thesis is to implement a new method of detecting particles contributed by the tungsten LPCVD system and to correlate this method to the existing defect detection tool. Secondly, the optical defect levels for tungsten will be compared to other steps in the backend process sequence and correlated to electrical defect levels. Thirdly, a technique will be established to identify and characterize defects on tungsten films. Finally, the particles will be classified both by defect size and elemental composition.

1.3 Thesis Organization

Chapter 2 provides background information related to several aspects of the project. First, several types of defect identification techniques are described. Next an overview of statistical process control is given followed by the basic theory of laser-based particle detectors. The chapter ends with an overview of the tungsten chemical vapor deposition system.

Chapter 3 describes how a new laser-based contamination analyzer tool was established in order to monitor optical defects added by the tungsten CVD process and equipment. Control limits, baseline particle levels and trend data for the new and existing monitor tools are compared and correlated in order to identify an effective station level monitoring technique.

Chapter 4 correlates optical defects to electrical defects from each step in the backend process. The relative number of optical defects added by each step is also compared.

Chapter 5 investigates process and equipment related particle sources within the tungsten deposition system.

Chapter 6 presents a methodology for establishing an effective particle detection and characterization program for deposited tungsten films. Particle detection and elemental characterization strategies are optimized by investigating the material properties of tungsten films.

Chapter 7 presents the particle characterization results for blanket film and no reactive gas flow (bare silicon) monitors. Relevant defect paretos, trends and elemental particle compositions are analyzed as well as matched to chamber hardware particle sources.

Chapter 8 presents the findings from this research and recommends future work.

Chapter 2
Background

2.1 Defect Identification

2.1.1 Introduction

In order to for a company to be competitive and maintain market share it must be able to manufacture its products in high volume at the lowest possible cost. In order to attain these goals the semiconductor world has trended towards smaller feature sizes, larger wafers and technological advances such as multilevel interconnects. Such trends pose great challenges to the fabrication defect-free integrated circuits. With multilevel interconnect technology, several process sequences are repeated for each metal layer creating the potential for defect multiplication. In addition, the downward trend in device dimensions increases the yield killing potential of smaller and smaller defects, figure 2.1. Moreover, the desire to pack more devices on a chip has created an upward trend in chip size which increases the probability of defects falling on a given die, figure 2.2.

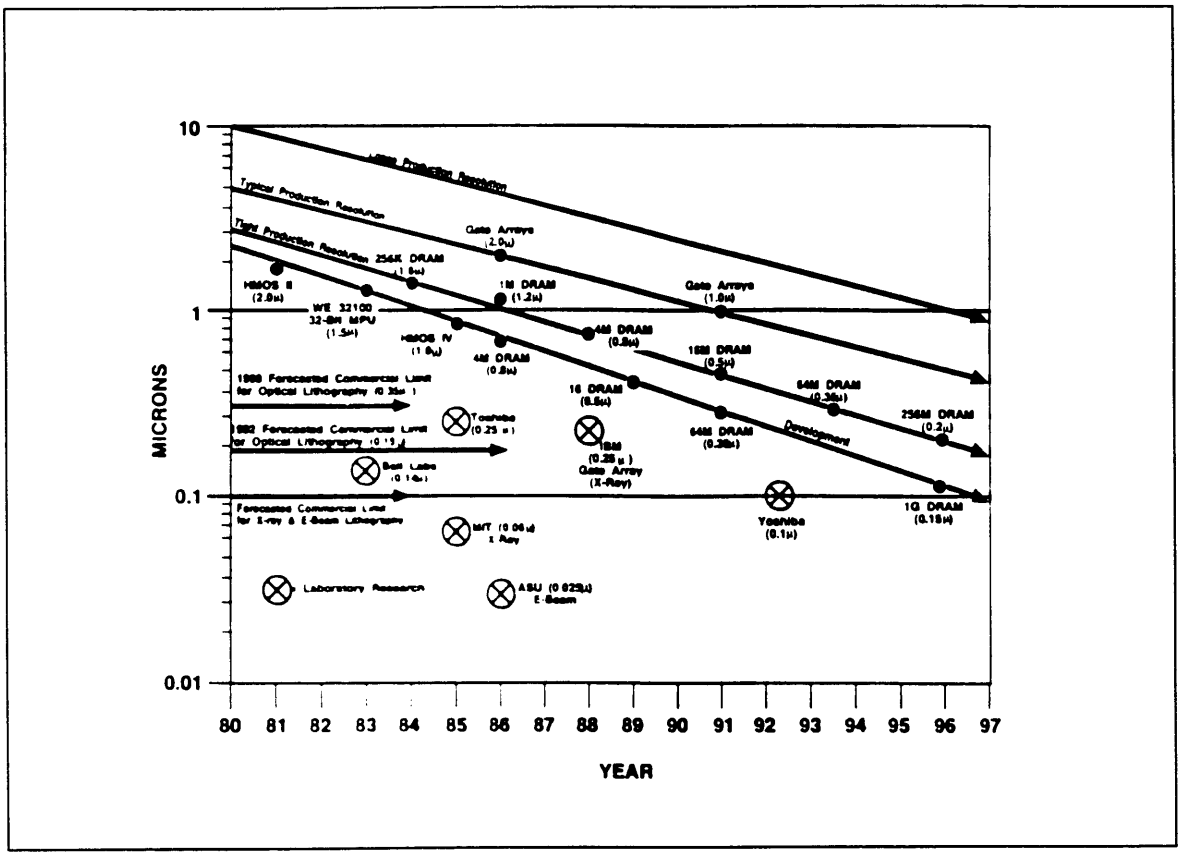

Figure 2.1 Device feature size trend due to scaling.

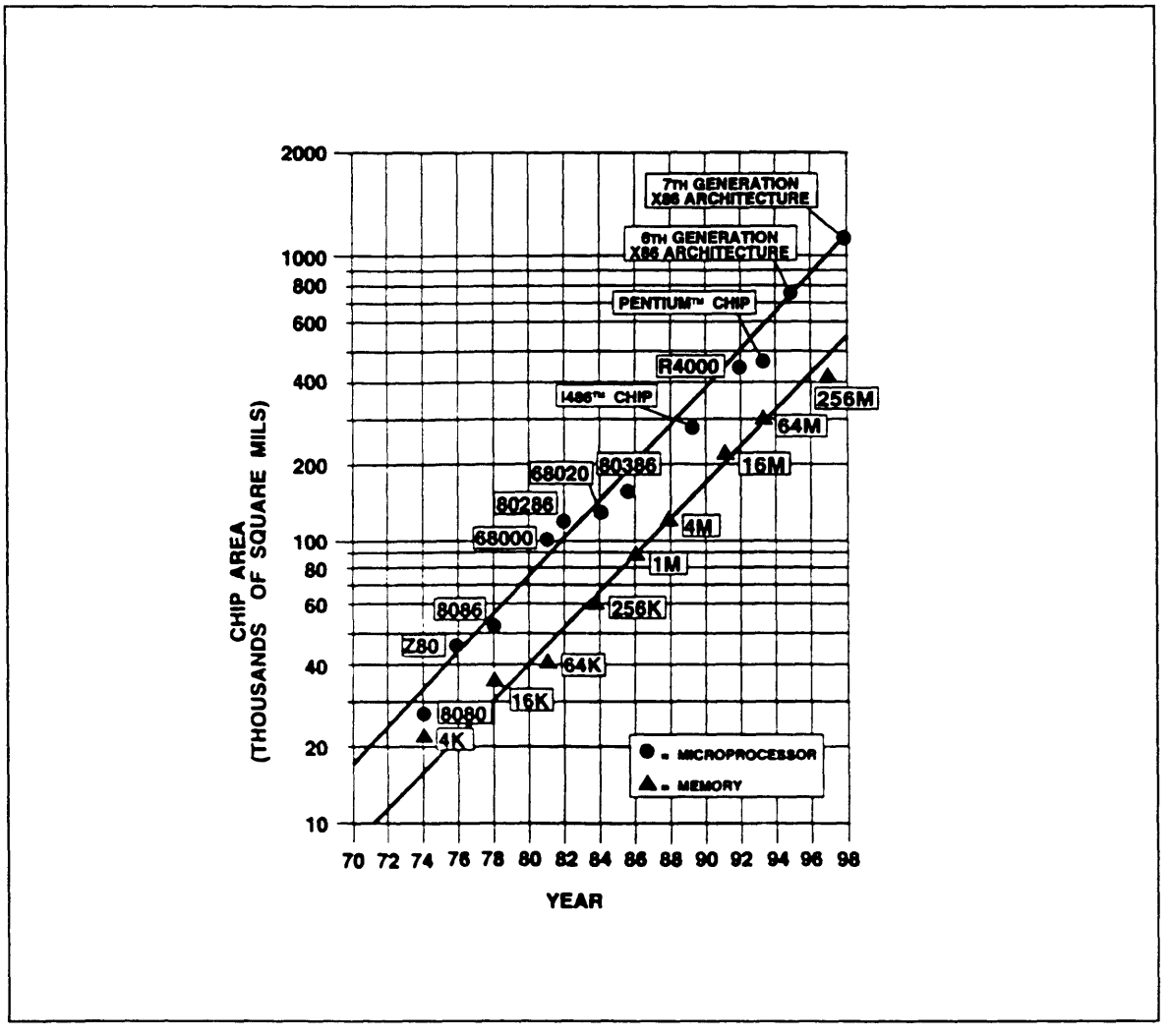

Figure 2.2 Die size trend.

Driven by manufacturing goals of lower cost and higher yields and challenged by the market trends, the goal in defect metrology is to achieve zero defects and 100 percent yield; however, this case is rarely achieved. Realistically, every step in the process flow is subject to defects which may reduce yields. The two types of defect related problems facing integrated circuit processing are reliability failures which are captured in the field and e-test and sort failures which are identified by the manufacturer.

2.1.2 Reliability Defects

Defects causing reliability problems are perhaps the worst type, as they have the greatest impact on customers. Despite the great delay in information feedback with field returns, failure analysis methods can be applied to the part in order to determine the failure mechanism. Such failure mechanisms may be traced back to either assignable or random problems with the process. However, a preferred method of identifying these defects is to test the reliability of the product before shipping it to the customer. Accelerated reliability testing of products gives a faster look into the quality of the product and can provide valuable information on the defect's interaction with the environment. Unfortunately, reliability testing requires the product to be fully processed and packaged which can mean weeks or months before a failing product can be identified.

2.1.3 Yield Vehicles

Product yield levels can also identify defect levels since yield is exponentially proportional to the inverse of the defect density. A standard model used in industry for

yield to defect density is Seed's model, given by equation 2.1. Seed's model assumes that the defect density is nonuniform across the wafer and from wafer to wafer.

$$Y = e^{-\sqrt{DA}} \tag{2.1}$$

where D is the defect density and A is the critical area.

Yield vehicles can benchmark a process compared to other processes or even different manufacturing sites. For example, yield for a four inch wafer, 1.2 micron feature size memory process may be compared to the same memory process on eight inch wafers with a 0.5 micron feature size. However, the turnaround for yield vehicles is very slow as the product must be completely processed and electrically tested before any information can be gained.

2.1.4 Short Loops

Short loops are a shorter version of the overall process flow. Short loops can be very beneficial in identifying the electrical defect density of only a section of the process. For example, a backend short loop may start at a dielectric layer and continue through the first metal stack. The metal stack is then patterned into a serpentine test structure and electrically tested for defect-induced opens or shorts. The throughput time on these loops is much faster than for a complete product, though they are still not very effective at identifying real time variations in defect levels.

2.1.5 Monitors

Inline automatic defect inspection tools provide immediate feedback on defect densities. For example, laser-based contamination analyzers can provide information on defect levels, sizes and spatial coordinates which can be useful in identifying particulate sources. Properly placed inline defect inspection tools can be very effective at capturing particle excursions. Once an excursion is identified, the production line is stopped and the suspect process equipment is modified until the defect levels return to normal levels. Such an inline inspection program prevents good material from being processed through an out of control process.

Two common inspection methods include wafer-based and time-based monitoring. In the wafer-based monitoring, the particle monitor is run after every specified number of wafers whereas in the time based monitoring scheme the monitors are run after a certain period of time such as every day or shift. In either case, such inline inspection methods prove to be very cost effective by identifying near real time defect levels.

2.2 Statistical Process Control

2.2.1 Background

The concept of statistical control of a process sequence was introduced in 1924 by Walter A. Shewhart of the Bell Telephone Laboratories [Shewhart, 1986]. Statistical process control (SPC) was developed to better understand the inherent variation within process equipment and to use the variation as a guide to determining if/when the process is not in control. Variation occurs naturally in almost every process. By reducing variation there are many benefits including predictable and improved die yield, improved quality, lower costs and greater profits. Sometimes, however, a process can change due

to assignable causes, such as significant environmental changes, miscalibrations, variability of raw material, or human error. Assignable causes make a process unpredictable and cause it to loose the state of control. The objectives of SPC are twofold: 1.) To detect the presence of an assignable cause so that it can be corrected and 2.) To benchmark the process giving a reference for future process improvements.

In order to assure the integrity of the final integrated circuit, the tungsten deposition process must monitor key film characteristics such as thickness, uniformity, reflectivity and particles. Analysis of the film characteristics using Statistical Process Control methods can help in the timely detection of costly process shifts. One way to better understand and reduce the causes of variation is by using SPC graphical tools such as Ishikawa's Seven Tools: 1.) Brainstorming/Cause and Effect, 2.) Check Sheets, 3.) Trend Charts, 4.) Pareto Diagrams, 5.) Histograms, 6.) Scatter Diagrams and 7.) Stratification. The main tools which I use in my work are control (trend) charts, pareto diagrams, histograms, scatter diagrams and stratification.

2.2.2 Control Charts

A control chart is a trend chart with statistically determined control limits. The objective of control charts is to identify special causes of variation which indicate that a process has gone out of statistical control. A process is stable if it has a predictable distribution and is random in behavior over time. Control charts used in conjunction with probability plots can determine if a normally distributed data set is in or out of control.

Traditionally, the upper and lower control limits are set by determining the mean and standard deviation.

Upper control limit (UCL) = Mean + 3 sigma

Lower control limit (LCL) = Mean - 3 sigma

In a manufacturing environment a variety of processes result in non-normal distributions. Examples are yields and contamination counts. The basis for this work is in particle reduction and, unfortunately, traditional statistics can not be applied to particle data because defect data often violate the Identically, Independently and Normally Distributed (IIND) basis of SPC. However, control limits can still be established for particle data by transforming the data.

The method of determining control limits for particle data is:

1. Create a trend chart.
2. Look for trends, shifts and repeating patterns
3. Construct a probability plot, figure 2.3. Since particle data is rarely normal, a square root transformation may be necessary.
3. Identify and delete outliers
4. Draw a smooth curve.
5. Find the 99th percentile to establish the upper control limit (UCL), figure 2.4.
6. Lower control limit (LCL) = 0

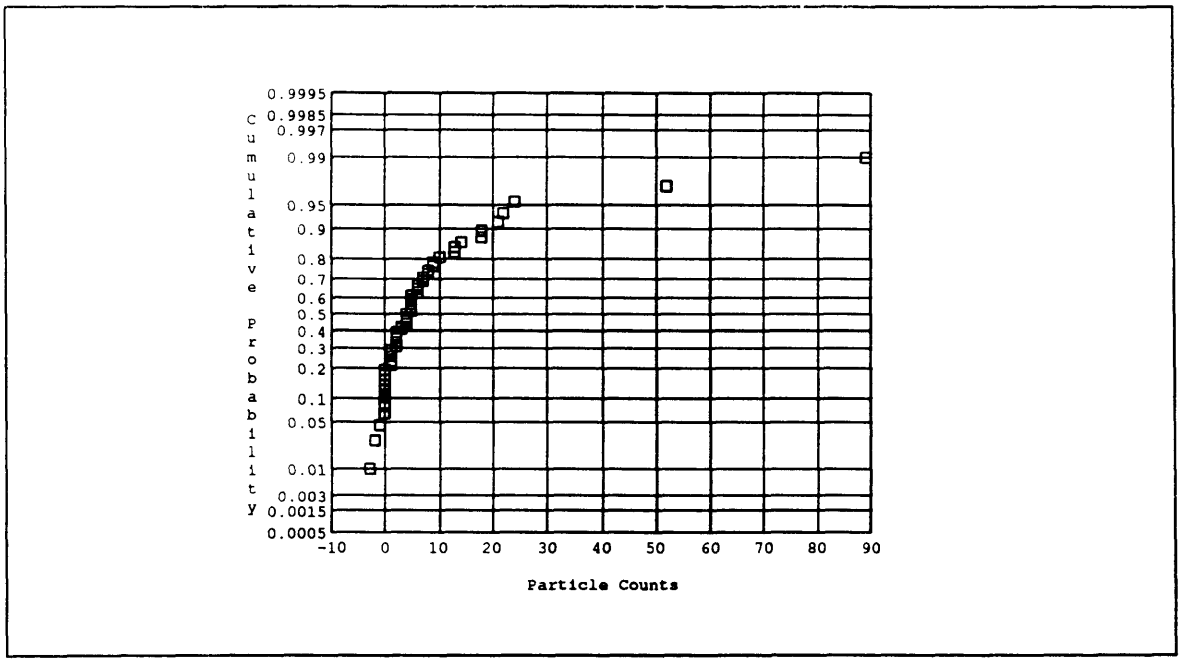

Figure 2.3 Particle Probability Plot.

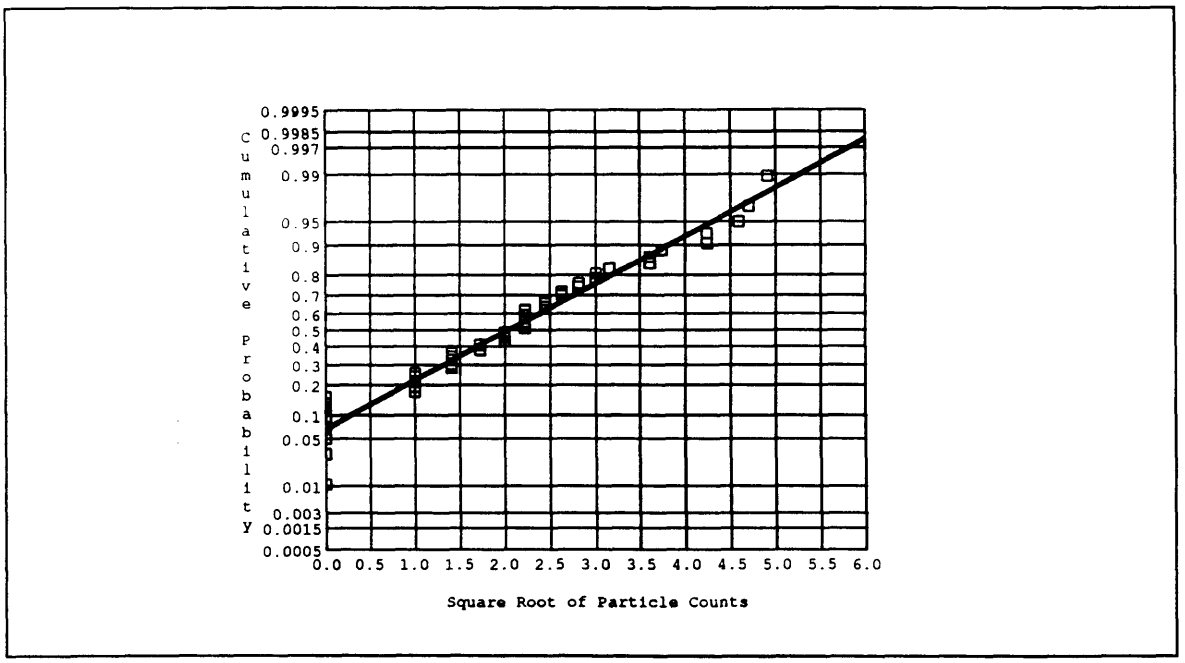

Figure 2.4 Upper Control Limit established at 99th percentile.

2.2.3 Pareto Diagrams

Defects can be identified according to both their size and frequency. As feature sizes decrease, smaller and smaller defects impact the yield making it increasingly important to identify the nature of particles. The nature (size, shape, elemental makeup, etc.) is important as it helps identify the source of the problem. Defect pareto diagrams are an excellent graphical tool to observe the progress of defect reduction efforts and also to direct valuable resources to addressing the highest leverage defect types. Figure 2.5 shows a sample pareto diagram indicating the electrical defect densities associated with different defect types.

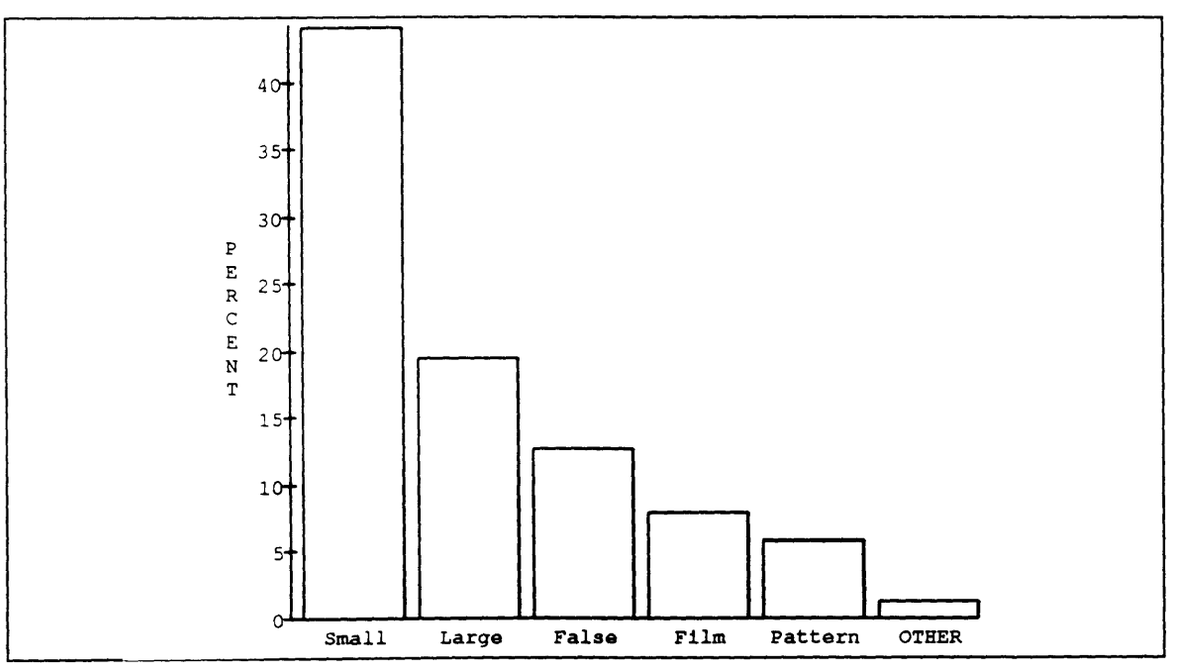

Figure 2.5 Electrical defect density particle pareto.

2.2.4 Histograms

Histograms are a useful tool which provide a graphical display of the distribution of measurement data. Histograms give us information about the amount of variability a collection of measurements has as well as the distribution shape and center point. Figure 2.6 shows a bimodal frequency distribution for particle counts. In this case, the existence of two peaks may indicate two distinct particle failure types.

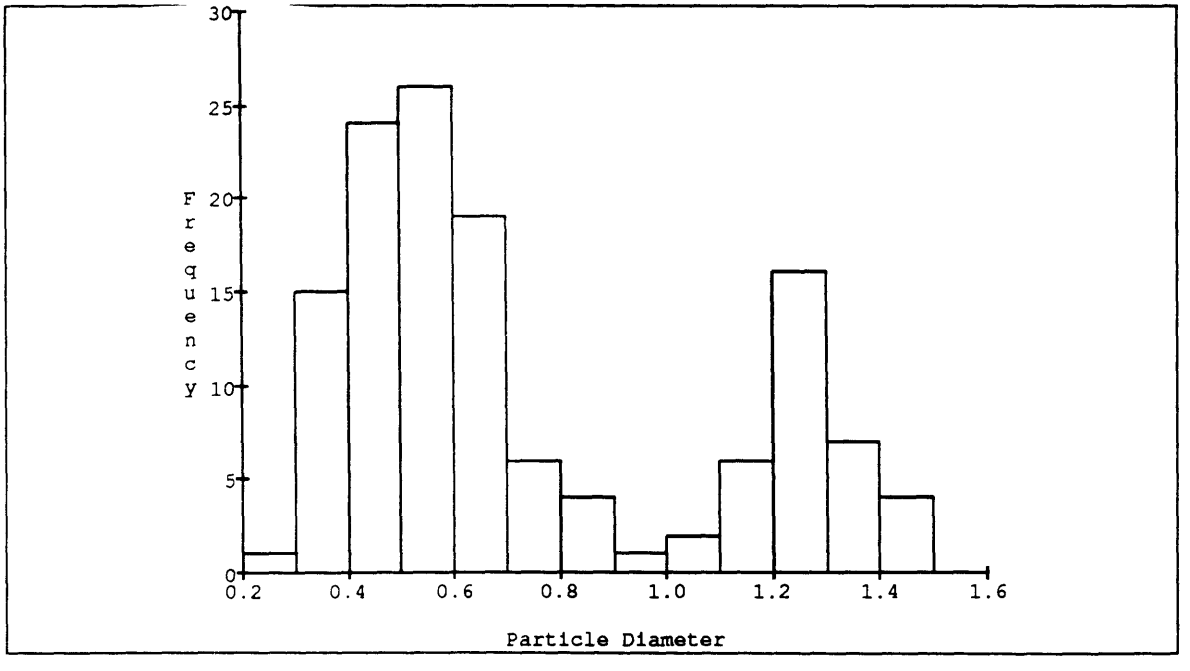

Figure 2.6 Particle sizing histogram.

2.2.5 Scatter Diagrams

Scatter diagrams are graphs that display the relationship of one variable versus another. Scatter diagrams are useful when correlating different variables. Figure 2.7

shows the particle counts versus film thickness. In this case, there is no correlation between particle counts and film thickness.

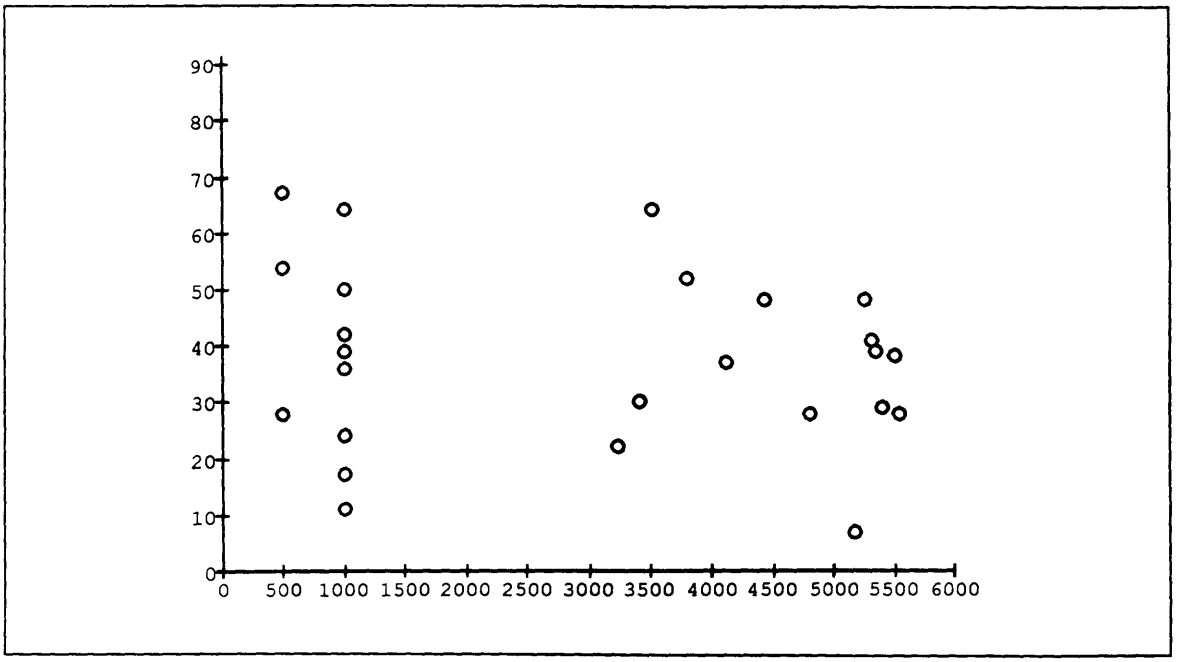

Figure 2.7 Scatter diagram of particle counts versus film thickness

2.2.6 Stratification

Stratification is the process of separating observations into meaningful groups in order to determine whether there is a variational source of difference. Many SPC tools such as histograms, scatter diagrams and trend charts can be stratified to better understand the data. Figure 2.6 shows a histogram displaying a bimodal frequency distribution in particle sizes. Optical and elemental characterization of these two modes may indicate two separate defect types. Stratification can also be useful in detecting sources of variation such as different chambers, operators or time of day.

2.3 Laser-Based Contamination Analyzers

2.3.1 Background

Manufacturers of Integrated Circuits widely employ laser wafer scanners for the detection of surface contamination. Laser wafer scanners can gather data on both the number and size of the particulate contamination. Commercial instruments are generally very accurate at determining the number of particles larger than the detection threshold, however they perform marginally when used for particle sizing. This is because the scattering behavior for a particle in contact with a surface is a very complex phenomenon. In addition to particles, light is also scattered by voids and grain boundaries which contribute to the surface roughness of a film. A better understanding of the effects of surface roughness on particle detection can be gained by applying vector diffraction theories to optical scatter.

2.3.2 Vector Diffraction Theory

Given a metal film with a roughness much smaller than the wavelength of the scattered light, vector scattering theories describe the differential light scatter (dP) into solid angle element $d\Omega$ in the direction θ_s, ϕ_s from light incident at θ_i as:

$$\frac{1}{I}\frac{dI}{d\Omega} = \frac{16\pi^2}{\lambda^4}[\cos\theta_i \cos^2\phi_s Q(\theta_i,\theta_s,\phi_s,\chi_i,\chi_s)g(k)] \qquad (2.2)$$

where χ_i and χ_s are the incident and scattered polarization states, g(k) is the frequency spectrum of the surface roughness and k is the surface spatial frequency. Note that light scattering from a surface is proportional to λ^{-4} as in Rayleigh and Mie scattering. Light

scattering also depends on polarization and surface spatial frequencies. Figure 2.8 shows film surfaces with low and high spatial frequency.

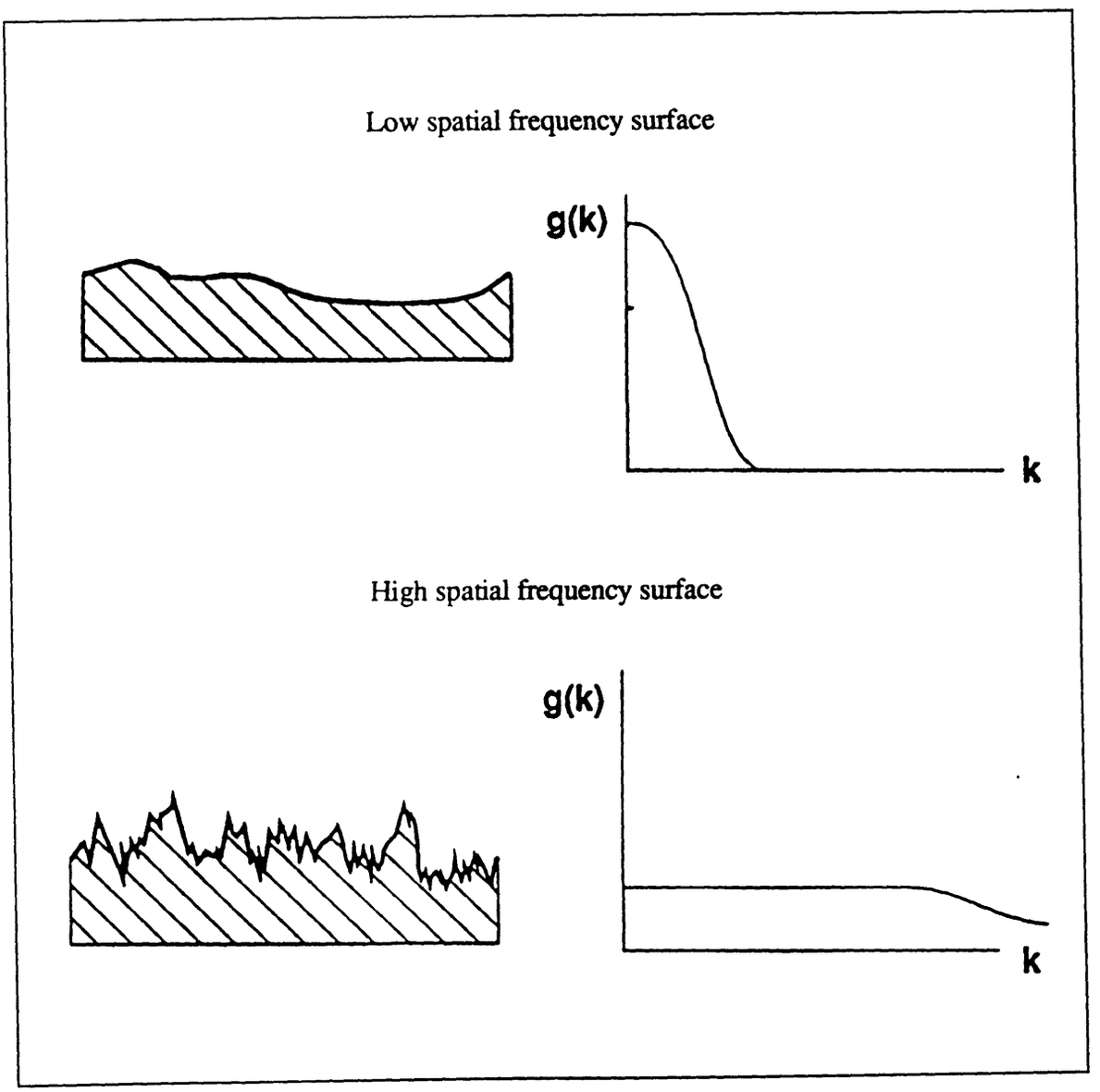

Figure 2.8 Comparison of low and high spatial frequency distributions of a surface.

2.3.3 Light Scattering and Surface Roughness

The most commonly used surface-finish parameter is the RMS roughness, σ, which depends on the range of surface spatial frequencies. Using vector scattering theories, it has been shown that the total integrated scatter (TIS) is related to the surface roughness. TIS is the integral of the angle resolved scatter that is obtained by using a reflecting hemisphere. Given no interferometric effects of the film, TIS is expressed in terms of surface roughness as [Church, 1979]:

$$\text{TIS} = \frac{\text{Total scattered light}}{\text{Total reflected light}} \tag{2.3}$$

$$= 1 - e^{(4\pi\sigma/\lambda)^2} \tag{2.4}$$

$$\approx (4\pi\sigma/\lambda)^2 \tag{2.5}$$

According to equation 2.5, scatter is strongly related to RMS surface roughness. Surface roughness not only adds to the background signal, it also reduces the amount of light scattered by the sphere into the detector. Since it is necessary for the particles to be seen above the background scatter of the substrate, conditions which produce minimal background scatter and high particle scatter optimize the detection process.

2.3.4 Contamination Analyzer Concepts

2.3.4.1 Measurement Concept

Figure 2.9 demonstrates the scanning technique used for detecting defect contamination on a substrate. A focused laser beam scans a linear at a specific angle of

incidence to the surface of the substrate. The substrate is moved at a constant velocity through incident beam and perpendicular to the line of scan in order to ensure that the entire surface is sampled by the beam. When the laser spot illuminates a defect on the surface, light is scattered away from the point of incidence. The scattered light is collected by the optical system and directed to a low-noise photomultiplier tube (PMT) for amplification. Both the collecting optics and the photomultiplier tube are essential to the tool operation as they control the two main operation parameters: the gain and collection threshold. The gain determines the relative amplification of the scattered light signal while the threshold sets the lower limit on the power of scattered light that is collected.

2.3.4.2 Detection Criteria

In addition to the expected scattering peak from a defect, there is a distribution of low amplitude pulses due to system noise and background scatter. In order to differentiate between the two, the signal pulses are compared to a threshold and rejected if they are less than this level. As long as the threshold is well above the noise level, the false count rate is zero. The threshold must then be placed so as to minimize false count artifacts and maximize real defect detection.

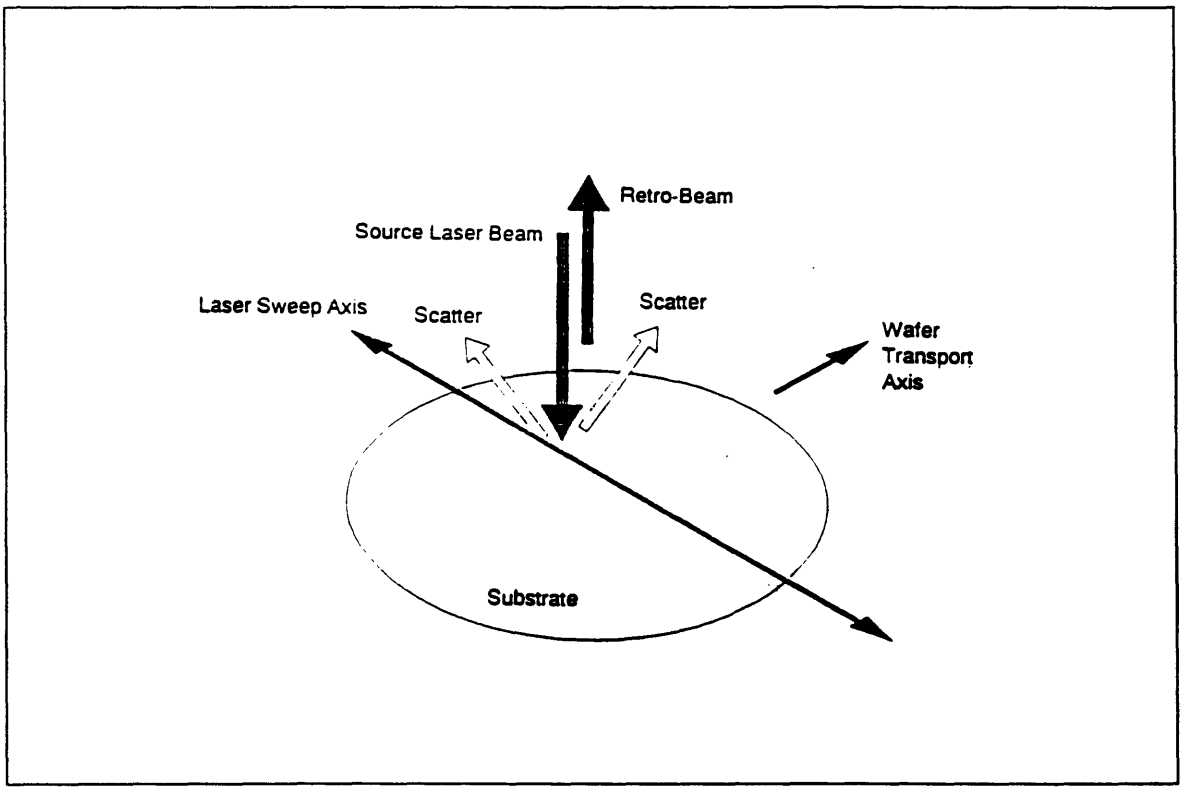

Figure 2.9 Scanning technique for detecting defect contamination.

2.3.4.3 Bare Wafer Contamination Analyzer

The bare wafer contamination analyzer is a commercially available laser based particle detector which operating at a wavelength of 488 nanometers and near normal beam incidence. The surface analysis instrument detects, counts and sizes defects as small as 0.1um on semiconductor substrate materials. The bare wafer contamination analyzer can be used to detect defects on blanket films; however, due to the optics it is more effective on smooth surfaces such as polished silicon and less effective on rough surfaces. Therefore, within this thesis, this tool will be referred to as the bare wafer contamination analyzer.

2.3.4.4 Blanket Film Contamination Analyzer

The blanket film analyzer is a commercially available laser based particle detector operating at a wavelength of 488 nanometers and at a 10° angle of incidence. The grazing incident angle as well as other optical and hardware elements make the blanket film analyzer very effective at detecting defects as small as 0.3 μm on rough surfaces [Tencor, 1993]. This surface analysis tool can detect defects on bare silicon wafers; however, it is not as sensitive as the bare wafer contamination analyzer. Therefore, within this thesis, this tool will be referred to as the blanket film contamination analyzer.

2.4 Tungsten Deposition Process

2.4.1 Tungsten Reactor Configuration

The tungsten deposition tool is a commercially available multi-chamber system. It is a single-wafer, cold-wall LPCVD reactor equipped with a loadlock wafer transfer chamber, figure 2.10. Wafers are automatically loaded face-up from the loadlock chamber onto the susceptor. The reactant and carrier gases are introduced through a showerhead from above the wafer. Figure 2.11 shows the cross-section of an individual process chamber denoting the key chamber parts including the blocker plate, showerhead, susceptor, wafer lift, and quartz window.

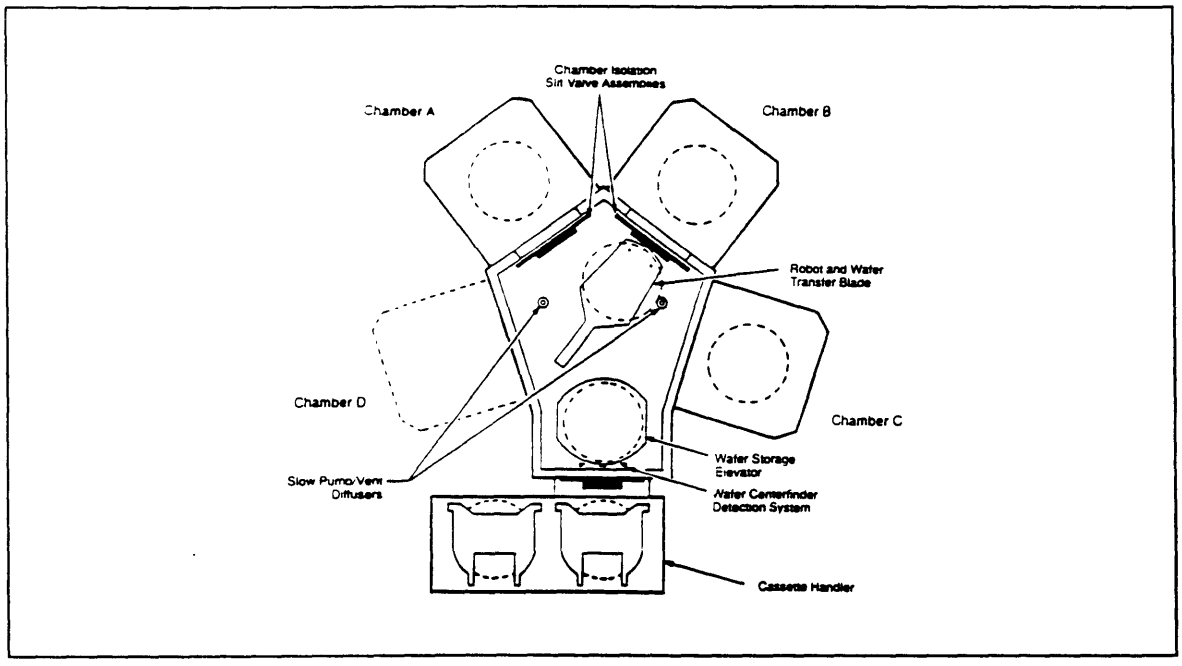

Figure 2.10 Tungsten chemical vapor deposition system

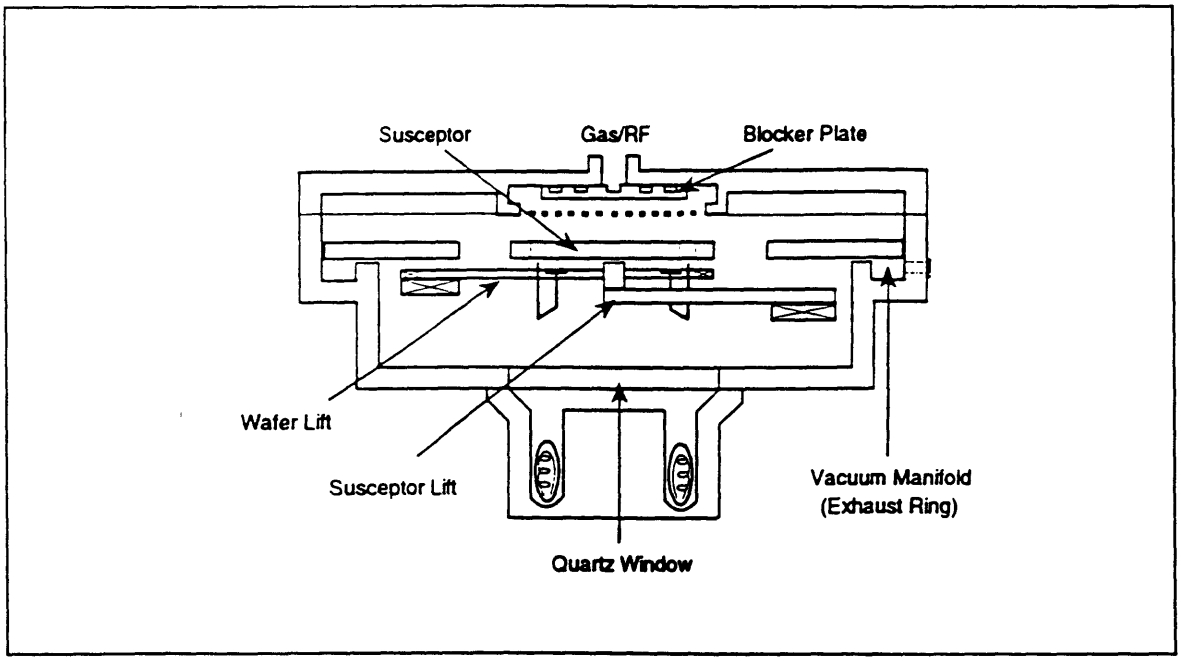

Figure 2.11 Schematic of the single wafer process chamber

2.4.2 Tungsten Deposition Process

The tungsten CVD process is divided into four sections: 1.) Nucleation Layer 2.) Bulk Deposition 3.) Backside Etch and 4.) Chamber Clean.

2.4.2.1 Nucleation Layer

The nucleation step places a seed layer of tungsten on titanium nitride (TiN). The starting substrate must be metallic otherwise the tungsten does not nucleate uniformly. Tungsten hexafluoride (WF_6) and silane (SiH_4) are used in this step since they nucleate readily on TiN. The reaction of WF_6 and SiH_4 has many reaction pathways, but the two most predominant reactions are:

$$3SiH_4 + 2WF_6 \rightarrow 2W + 3SiF_4 + 6H_2 \qquad (2.6)$$

$$2SiH_4 + WF_6 \rightarrow W + 2SiHF_3 + 3H_2 \qquad (2.7)$$

Since this reaction is a mass transport limited process, it does not provide good step coverage. Hence the nucleation step is kept short relative to the bulk deposition and only provides the first several hundred Angstroms of film.

2.4.2.2 Bulk Deposition

$$WF_6 + 3H_2 \text{ -----> } W + 6HF \qquad (2.8)$$

The bulk deposition step deposits 90% of the tungsten film. Due to the greater activation energy of H_2 reduced WF_6 compared to SiH_4, the hydrogen reaction does not readily nucleate on TiN and can not be used as a nucleation layer. For the process parameters used, the WF_6 and H_2 reaction is a surface limited reaction. Because of the reaction limited process, step coverage greater than 90% can be achieved. However, uniform temperatures must be achieved across the wafer as the deposition rate is very sensitive to temperature. Although the detailed mechanisms of hydrogen reduction on the surface is unknown, it is believed to be controlled either by activated H_2 adsorption or by activated desorption of HF [Hsieh and Joshi, 1992]. In the hydrogen reduction limited regime, the deposition rate has been found to be one-half order dependent on the partial pressure of H_2 with an apparent activation energy of 17 Kcal [Hsieh and Joshi, 1992].

$$\text{Deposition Rate} \propto P_{H_2O}{}^{0.5} \exp(-E_a / kT) \qquad (2.9)$$

2.4.2.3 Backside Etch

Since there is not a hermetic seal between the susceptor and the wafer during the nucleation and deposition stages, tungsten is also deposited on outer edge of the wafer backside. Consequently, the tungsten peels from the wafer as there is no adhesion layer on the wafer backside. To prevent peeling, a backside etch step is performed after bulk deposition. First, the wafer is raised up to the showerhead then a nitrogen trifluoride (NF_3) plasma is struck beneath the wafer. In addition to removing excess tungsten from the wafer backside, the etch process also removes tungsten from the chamber walls. The key reaction is:

$$6F + W \rightarrow WF_6 \qquad (2.10)$$

Since a relatively small percentage of the wafer backside has tungsten, only a fraction of the fluorine ions contained in the plasma are etching the tungsten from the backside of the wafer. Most of the fluorine radicals are etching the susceptor, chamber walls, pumping plate and other hardware components.

2.4.2.4 Chamber Clean

After backside etch, the wafer is removed from the chamber and returned to the loadlock. The next step is the chamber clean which removes any remaining tungsten in the system not removed by the backside etch. The chamber clean consists of two different steps. The first is an NF_3 plasma clean which focuses on cleaning the susceptor, showerhead and chamber walls. The second step is an H_2 plasma clean which neutralizes all fluorinated surfaces in the chamber.

$$H + F_{surface} \rightarrow HF \qquad (2.11)$$

The H_2 plasma clean scavenges the excess fluorine in the chamber. Without this clean, remnant fluorine atoms would react with SiH_4 during the subsequent wafer's nucleation step yielding an inadequate film.

Chapter 3
Tungsten Particle Monitoring

3.1 Introduction

Overcoming yield problems associated with multilevel interconnects is an extremely important activity because the value of silicon wafers increases as they progress toward the backend of a process flow. Defects may lead to the loss of a significant number of dice or wafers which have accumulated a potentially high market value. With such a high price for defect reduction, defect monitoring procedures must be carefully designed and implemented.

3.2 Establishing a Blanket Film Contamination Analyzer

3.2.1 Background

Presently particles are monitored on the tungsten system by exposing a bare silicon wafer to the process sequence without any reactive gas flow. After process exposure the bare silicon wafer is analyzed for light scattering defects using a laser-based contamination analyzer. A preferred method would be to monitor particles with the reactive gas flows on

since the resulting blanket tungsten film is more representative of the production wafer process sequence. However, the ability to detect small particles on inherently rough surfaces such as tungsten has only recently been developed.

The first step in implementing the blanket tungsten film monitor tool is to set up and verify a recipe which optimize the tool parameters for the desired film. Next, the particle levels need to be tracked over a period of time in order to establish baseline particle levels as well as control limits. Once baseline particle levels and control limits are established the blanket film monitor particle data is compared to the bare wafer particle monitor data in order to determine which tool is a more effective station level monitor.

3.2.2 Recipe Setup

The two key parameters for recipe set-up on the blanket film analyzer is the gain and display threshold. The gain determines the relative amplification of the scattered light while the threshold sets the lower limit on the power of scattered light that is collected. Analysis of the defect counts as a function of the display threshold yields an exponentially decaying plot. Figure 3.1 shows the plot for normalized particle counts as a function of display threshold for a tungsten film at different gain settings. The vertical line indicates where added particle levels drop off. To the left of this line, the particle counts are caused by scatter from the surface roughness and are not real defects. To the right of this line the defects are assumed to be real. In order to verify the validity of the defects and to identify the threshold particle size, microscopic review and latex sphere analysis must be performed.

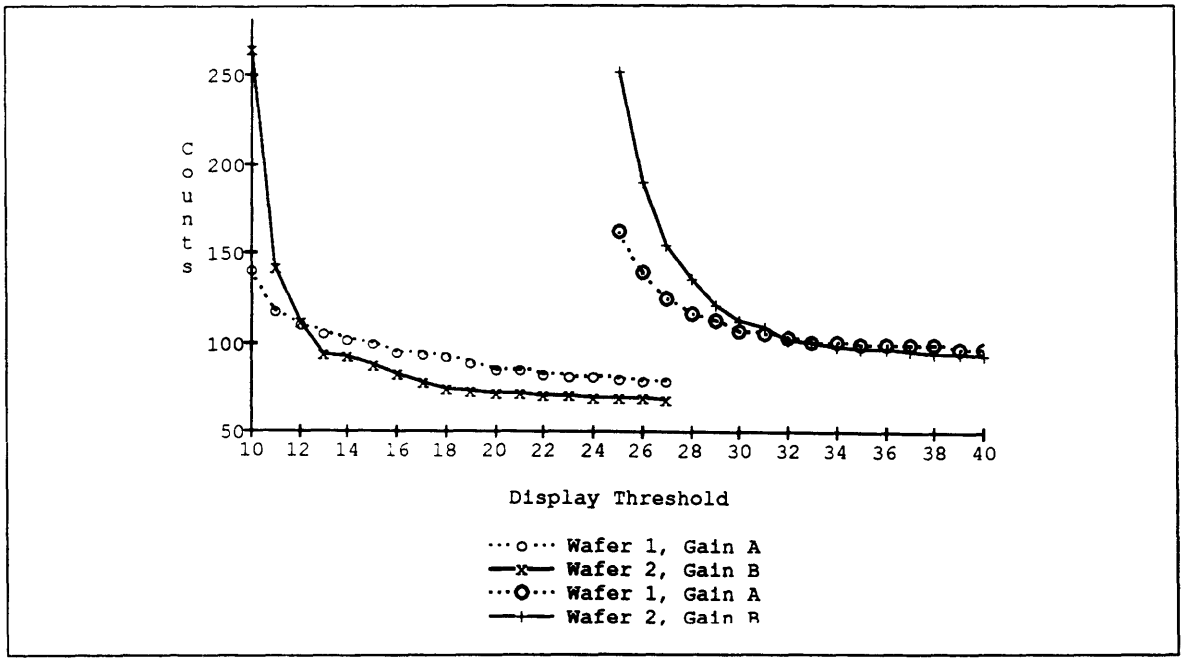

Figure 3.1 Normalized particle counts as a function of display threshold.

3.2.3 Recipe Verification

The recipe was verified by microscopically reviewing several tungsten film wafers and identifying the defect map failure sites as either valid or false defects. Using a real defect criteria of 95% the validity of the recipe was established.

To identify the detection threshold of this recipe, mono-disperse latex spheres of size 0.5, 0.8, 1.0 and 3.0 microns were deposited on separate production thickness tungsten films. Figure 3.2 shows the particle distribution curve for 0.5 micron spheres. Smaller spheres were not available, so a minimum detection threshold of 0.4 microns was extrapolated for production thickness tungsten films. By comparison, the bare wafer particle analyzer can detect spheres as small as 0.2 microns on bare silicon yet can not identify spheres as large as 3 microns on blanket tungsten films.

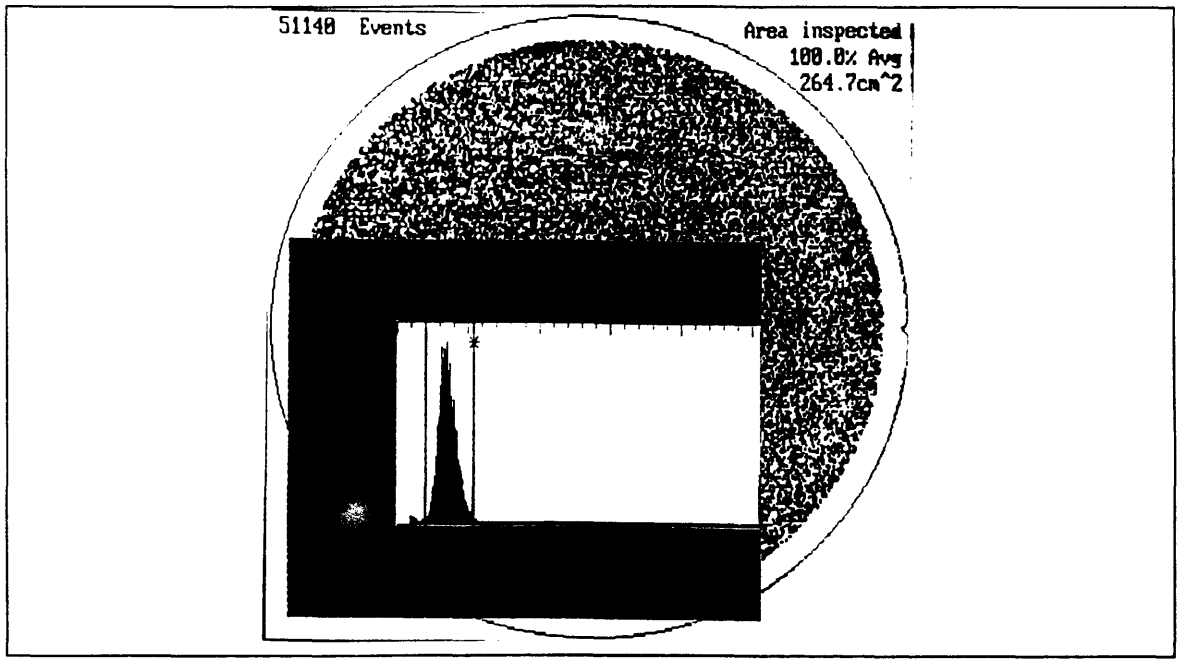

Figure 3.2 Particle distribution curve for 0.5 micron latex spheres.

3.3 Correlating Contamination Analyzers

3.3.1 Procedure

Particle data from a wafer-based monitor scheme was collected over a time span of four months yielding over 100 data points for each of the four chambers, A, B, C and D. Pre-deposition particle counts were recorded and subtracted from the post processing particle counts in order to determine the delta particle counts. The monitoring sequence is first a blanket film deposition wafer followed by a wafer which does not experience the reactive gas flow (bare wafer).

3.3.2 Results and Discussion

3.3.2.1 Baseline and Control Limits

Baseline and upper control limits were calculated for both the bare wafer and blanket film monitors using the rules described as in section 2.2.1. Table 3.1 shows the resulting normalized baseline and upper control limits. All four tungsten chambers have similar baseline particle levels for both the bare wafer monitor and the blanket film monitor. Likewise, the upper control limits for all chambers were roughly equivalent for both the bare wafer and blanket film monitor.

Table 3.1 Normalized Baseline and Upper Control Limits for the Bare Wafer and Blanket Film Monitors

Contamination Analyzer	Chamber Identification A	B	C	D	Average
Bare Wafer					
Baseline	0.20	0.20	0.23	0.17	0.20
Control Limit	1.00	0.87	1.00	0.87	0.94
Blanket Film					
Baseline	0.25	0.20	0.21	0.21	0.22
Control Limit	1.00	0.89	0.94	0.87	0.92

3.3.2.2 Trend Data

Particle excursions tended to fall into three different categories, small bin defects, cheerio pattern defects and bulls-eye defects.

Small Bin Defects The small bin defects were captured by the bare wafer monitor but not always by the blanket film monitor. Figure 3.3 shows a small bin defect excursion

map from the bare wafer monitor tool. The particle size-frequency histogram beneath the wafer map displays the excursion defects to range in size from 0.2 to 0.5μm with a peak size distribution at roughly 0.3μm. Since the blanket film monitor has a detection threshold of 0.4μm it appears that the blanket film monitor is not sensitive enough to capture these smaller bin defects.

Cheerio Pattern Defects In general, cheerio pattern defect excursions are captured by the blanket film monitor but not detected by the bare wafer monitor except in gross out off control excursions. Figure 3.4 shows the cheerio particle signature from the blanket film monitor. The cheerio signature is characterized by a dense circular defect pattern that is relatively clean near the center and edges of the wafer. The cheerio patterns have been traced to particles originating from the Constant Voltage Gradient (CVG) gas feed-through or showerhead. In the feed-through case, the reactive gases pass through the CVG where they react forming solid particles which reside within the gas line. During deposition, these particles are pushed through the line and deposit on the wafer. The cheerio pattern can also indicate degradation of the showerhead. In some instances where the chamber was opened during a cheerio excursion, a film build up was noted on the showerhead. During deposition the gas flows through the pores in the showerhead dislodge particles which then deposit on the wafer. Since the pores do not extend the full radial distance across the showerhead, there is a relatively clean zone near the edge of the wafer.

Bulls-eye Defect One disadvantage of the blanket film monitor; however, is that it often detects and magnifies defects not added by the tungsten system. Figure 3.5 shows optical photos of the Bulls-eye defect at different magnifications. In every case where the bulls-eye defect appeared, the defect could be traced to a pre-existing defect as identified

identified by the pre-scan particle map, figure 3.6 Bulls-eye defects have been identified as organic particles which outgas when heated during tungsten deposition. The outgassing poisons the area surrounding the defect creating a circular area several millimeters in diameter where no tungsten is present. This causes artificially high particle counts which triggers a false out of control. Fortunately, a technique has been established which can block out the bulls-eye defect area from the total particle count. This technique eliminates false out of controls and eliminates the need to run the particle monitor over again saving test wafers.

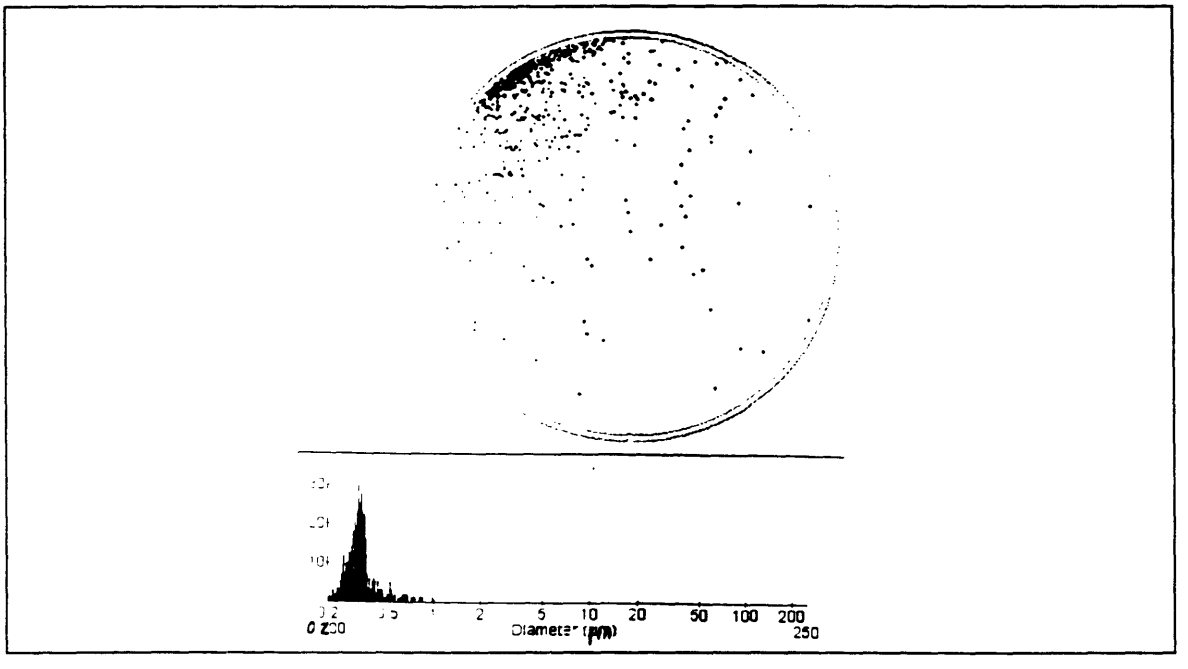

Figure 3.3 Small bin defect excursion map from bare wafer monitor tool.

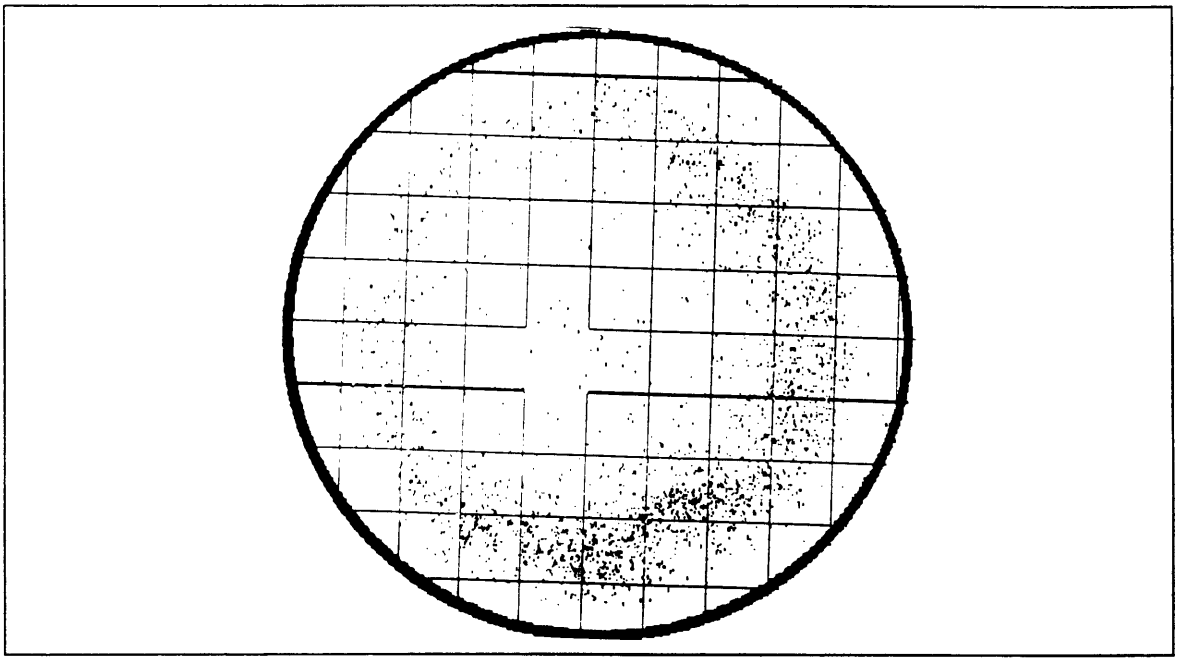

Figure 3.4 Cheerio defect pattern from blanket film monitor tool.

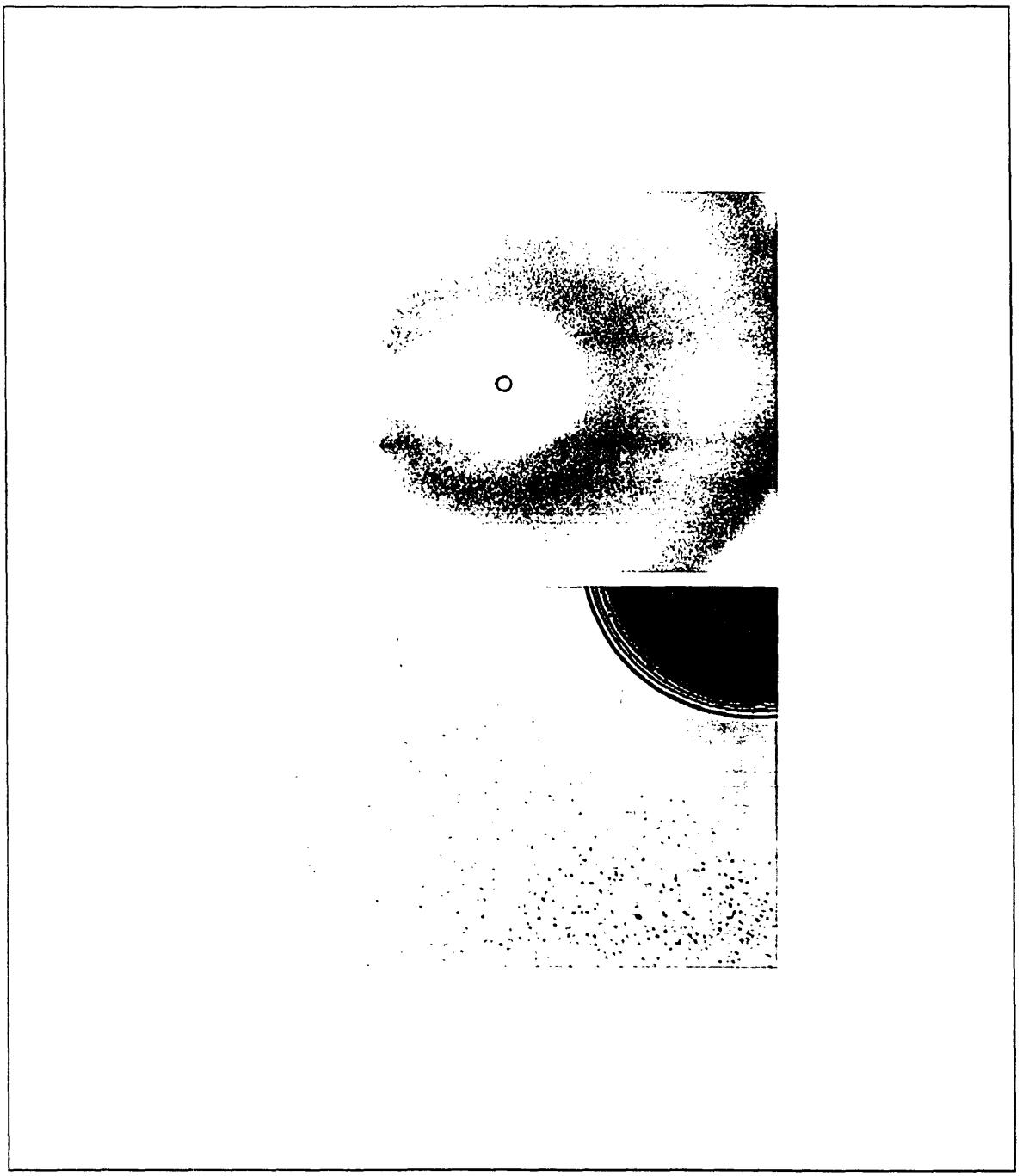

Figure 3.5 Optical photographs of the Bulls-Eye defect.

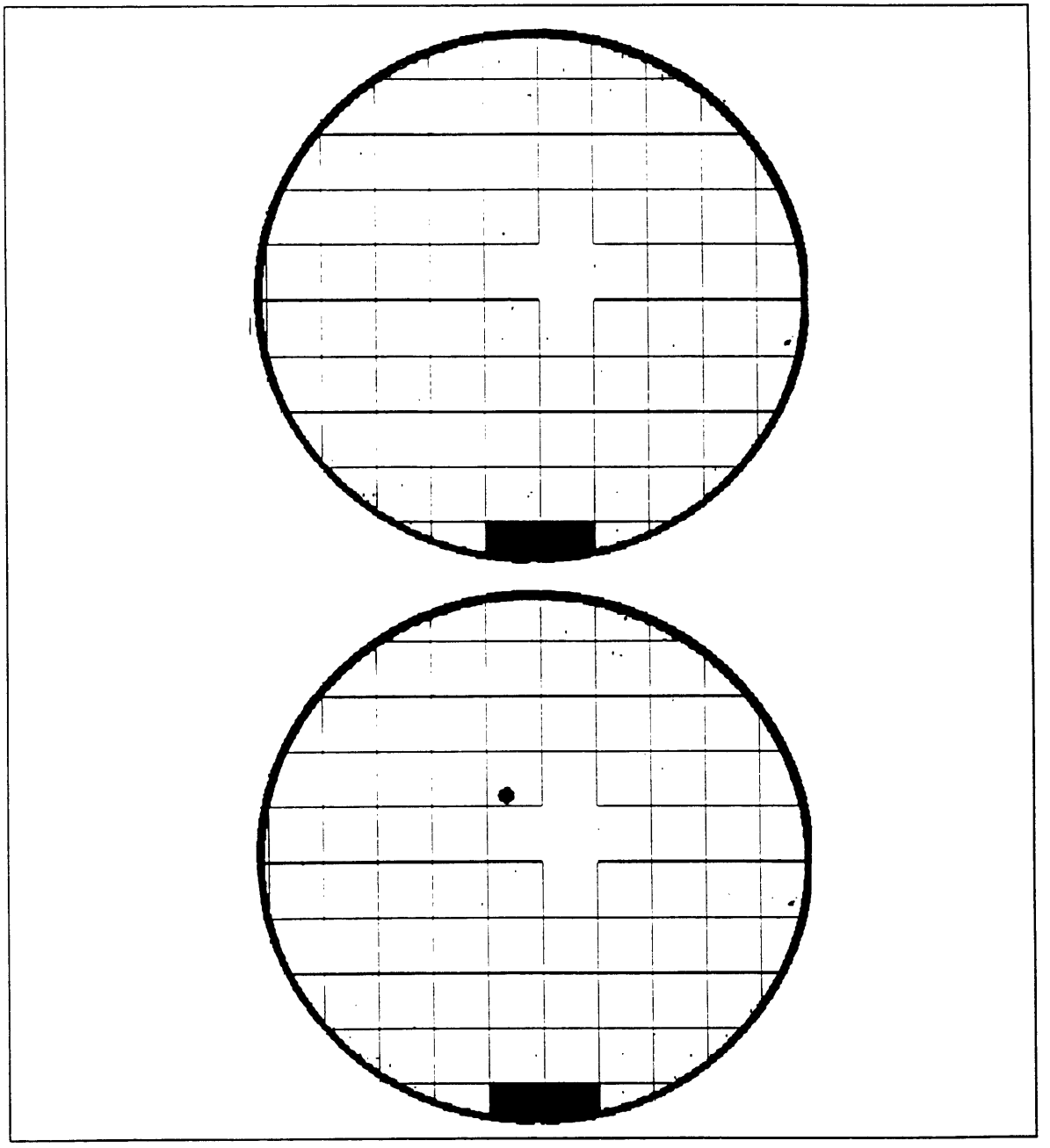

Figure 3.5 Pre and post-deposition deposition defect maps showing the Bulls-eye defect from blanket film monitor.

3.4.3 Conclusion

In summary, it appears that both monitor tools are necessary in order to capture defect excursions of every bin size and category. The bare wafer monitor is better adapted at identifying smaller defects while the blanket film monitor can better detect defects associated with the reactive gas flows (cheerio pattern).

Chapter 4
Optical-Electrical Defect Correlation

4.1 Introduction

The previous chapter dealt with implementing a new laser-based contamination analyzer as a monitor tool in order to more effectively control the tungsten module. An important point to realize is that these defects were optical defects and may not adversely affect yield. If possible, the visual defect should be correlated to an electrical defect in order to better understand the potential affects on yield. This can be achieved by electrical testing of backend short loop serpentine structures. The resulting open and short failures can then be microscopically reviewed and attributed to the defect causing process step.

4.2 Experimental Procedure

4.2.1 Process Sequence

A short loop process sequence was initiated that covered part of the backend metallization process. First borophosphosilicate glass was deposited in order to isolate the underlying bare silicon from the serpentine structure (not yet defined). Next a titanium

nitride film was sputtered as an adhesion layer for subsequent blanket tungsten deposition and etchback. Note that the titanium nitride/tungsten/tungsten etchback sequence (integrated tungsten plug module) is non-value adding since no contacts or vias were patterned; however, these steps were included in order to determine the defects added by the integrated tungsten plug module. After tungsten etchback, the metal 1 (M1) stack is deposited and patterned into the serpentine test structure. The serpentine structure has linewidths and spaces comparable to production feature sizes in order to better simulate the electrical defect failure mechanisms. Figure 4.1 shows a sample serpentine structure.

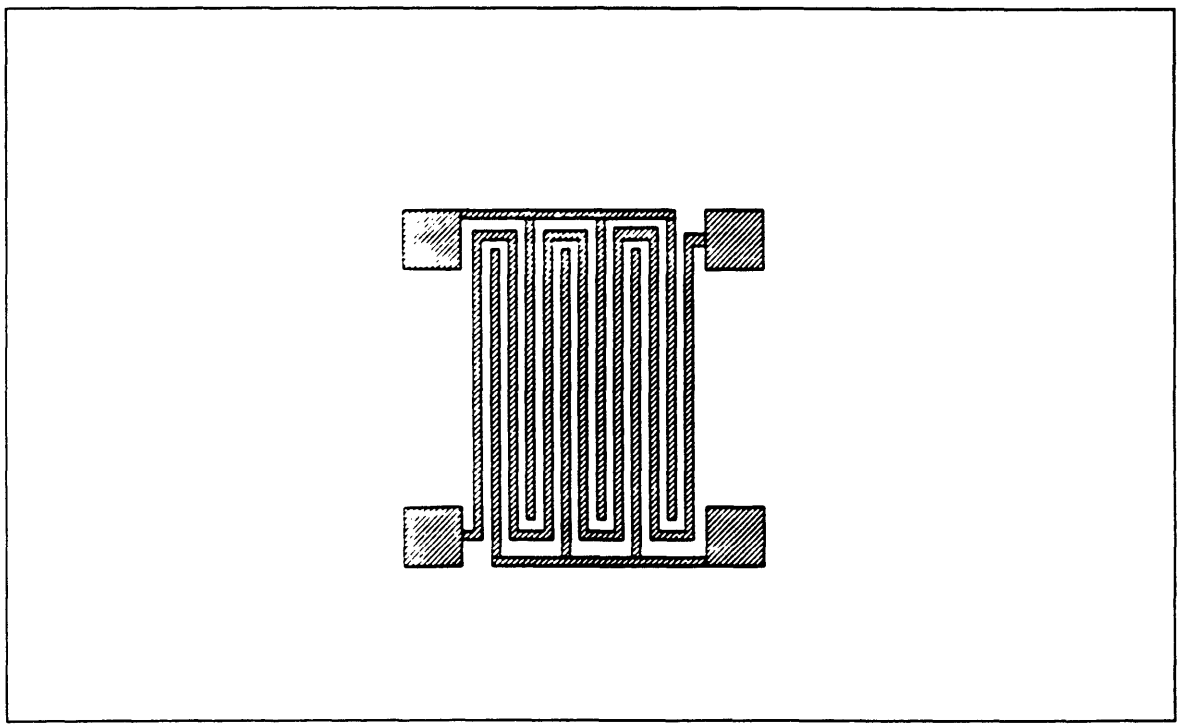

Figure 4.1 Serpentine electrical test structure.

4.2.2 Particle Tracking

A laser-based, blanket film contamination analyzer detected light scattering defects at each successive step: BPSG, TiN, W, W etchback and AlCu. Light scattering defect maps used in conjunction with overlay software allowed us to track the added, common and removed defects from step to step.

4.2.3 Electrical Testing and Characterization

After patterning the metal lines the test structures were electrically tested for opens and shorts. The electrical defect sites were then reviewed with an optical microscope and the defects were classified into eight categories: Large, Flake, Metal film, Probe error, Pattern, False, Scratch and Other. Representative defects were submitted for SEM/EDX analysis in order to determine the elemental composition.

4.3 Results

4.3.1 Particle Tracking

Using the blanket film analyzer defect maps, overlay software determined the added, removed and common defects at steps TiN, W, WEB and M1. Table 4.1 shows the data collected using the overlay software. Rows 1 through 4 show the statistical data for the added defects at each step. For example, the normalized particles added increased with each step: TiN 1, W DEP 2, WEB 4 AND M1 4. Row 5 shows the percent of pre-step defects that are present after processing. For example, 78.8% of all defects present after W deposition are detected after WEB. Row 6 shows the percent of the added

defects from each step which are still present and detected after M1 deposition. For example, 74.5% of the W added defects are present and detected after M1.

Table 4.1 Overlay software normalized data for serpentine short loop.

	TiN	W	WEB	M1
1. Median Particles Added	6	12	22	26
2. Mean Particles Added	7	20	36	32
3. Standard Deviation	4	18	35	18
4. Range	9	48	100	51
5. Percent Present after Next Step	85.6	78.8	79.7	-
6. Percent Present after M1	83.7	74.5	72.5	-

4.3.2 Electrical Testing and Characterization

Figure 4.2 contains the electrical defect pareto for the serpentine test structure short loop. Most of the defects fell into the large category followed by flakes, metal film, probing error, pattern, false and scratches.

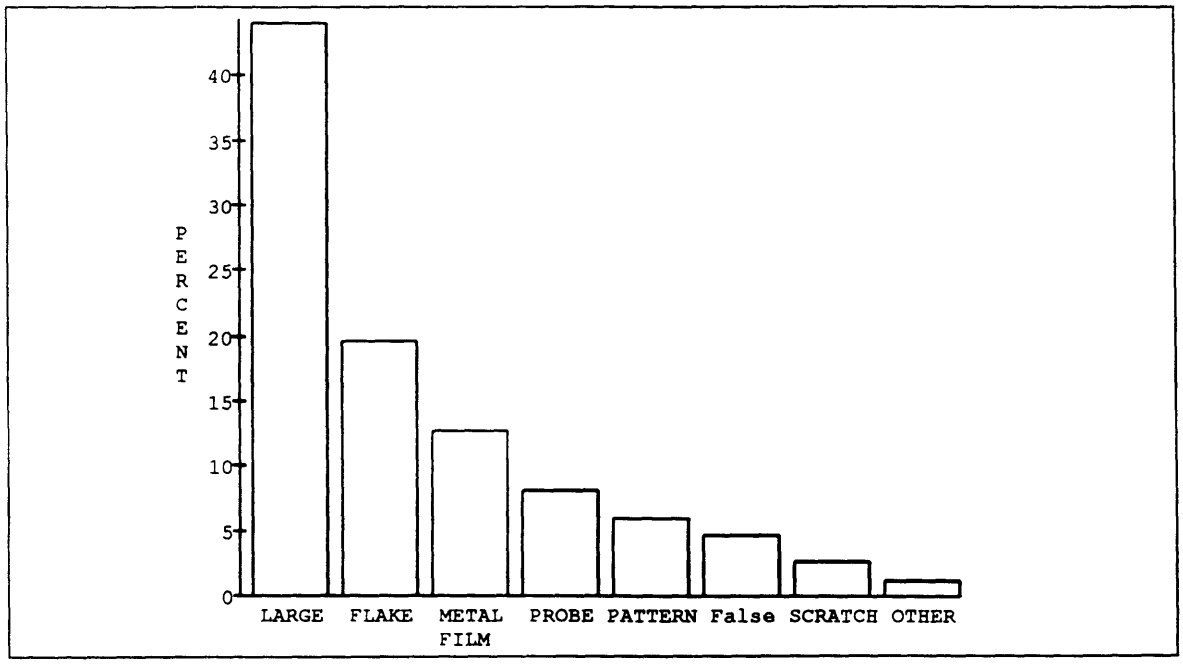

Figure 4.2 Electrical defect pareto diagram.

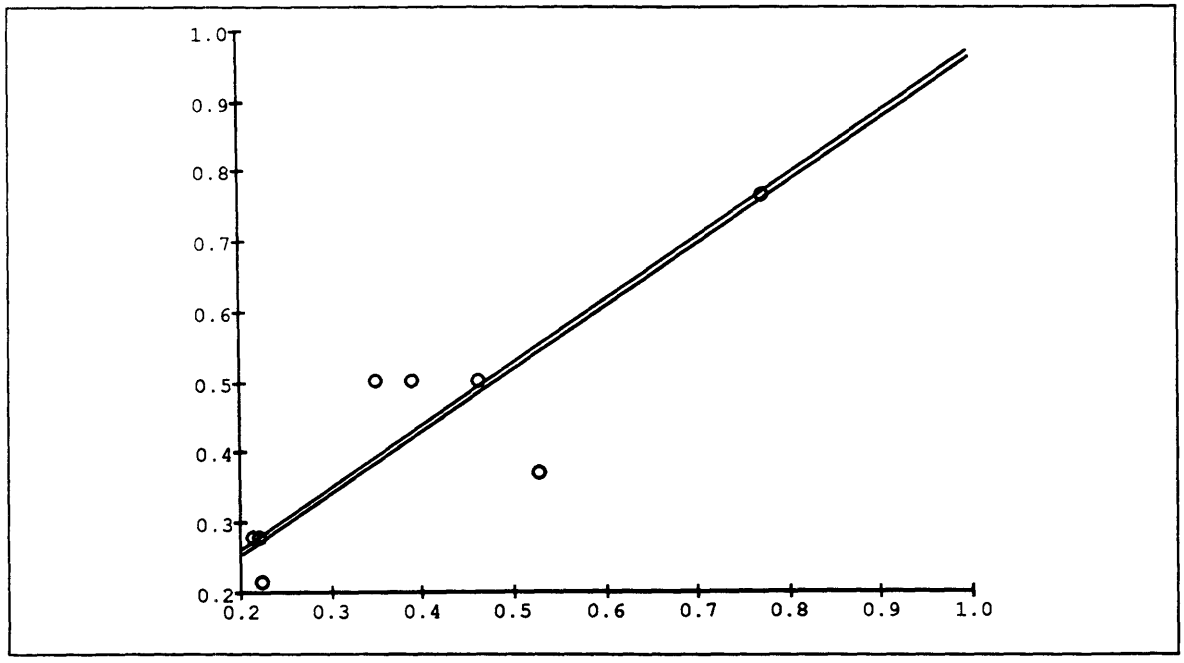

Figure 4.3 Normalized electrical defect density vs. total defects after M1 deposition.

4.4 Discussion

4.4.1 Particle Tracking

Figure 4.3 shows the strong positive correlation between the total defects detected after M1 deposition and electrical defect density. For each of the three highest E-test defect densities there were specific contributors to the overall particle levels. The highest electrical defect density case was caused by tungsten etchback which added 62.5% of the total M1 defects. Figure 4.4 shows the randomly distributed particle signature left behind by WEB. The second highest defect density was caused by M1 deposition which added 65.7% of the total M1 defects. Figure 4.5 shows the concentration of particles on the notch up left side of the wafer. The third highest defect density was caused by tungsten deposition which added 64.3% of the total M1 defects, figure 4.6.

4.4.2 Electrical Testing and Characterization

EDX analysis of representative electrical failures was unable to identify the elemental composition of the defects. The 15KeV electron beam, having a greater penetration depth and large interaction volume, went right through the particles and gave the same particle signature as the background signal. The 5KeV beam, on the other hand, did not have enough potential to identify some of the more dense elements. The wide number of elements identified in the background signal (Boron, phosphorous, silicon, oxygen, titanium, aluminum and nitrogen) overshadowed the particle's elemental signature causing characterization to be very difficult.

Focused Ion Beam (FIB) analysis could have been used to strip back the films order to pinpoint the exact layer and enhance elemental characterization, however the resources were limited and FIB work is very time consuming.

4.4 Conclusion

Defects present at any of the steps (TiN, W, WEB) have roughly the same chance (80%) of being present and detected at the next step (W, WEB and M1 respectively). Similarly, defects added by any of the steps (TiN, W, WEB) have roughly the same chance (75%) of being present and detected after M1 deposition. Therefore, placing an inline defect monitor for production wafers after M1 deposition would be an extremely effective method of detecting particle excursions at all of the backend process steps prior to and including M1 deposition. The strong correlation between defects detected after M1 deposition and electrical defect density further strengthens the placement of an inline defect monitor at M1. Though being an effective particle monitor, SEM/EDX analysis of particles after M1 deposition is ineffective at identifying the unique elemental composition of the defect.

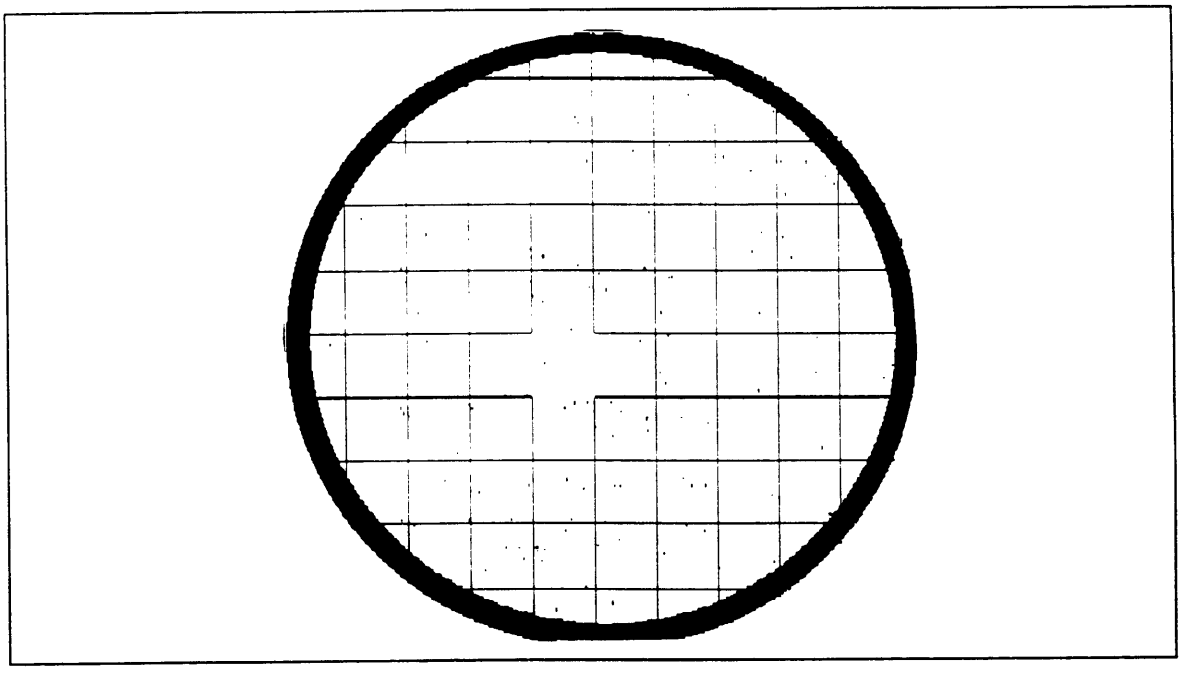

Figure 4.4 Randomly distributed WEB particle signature.

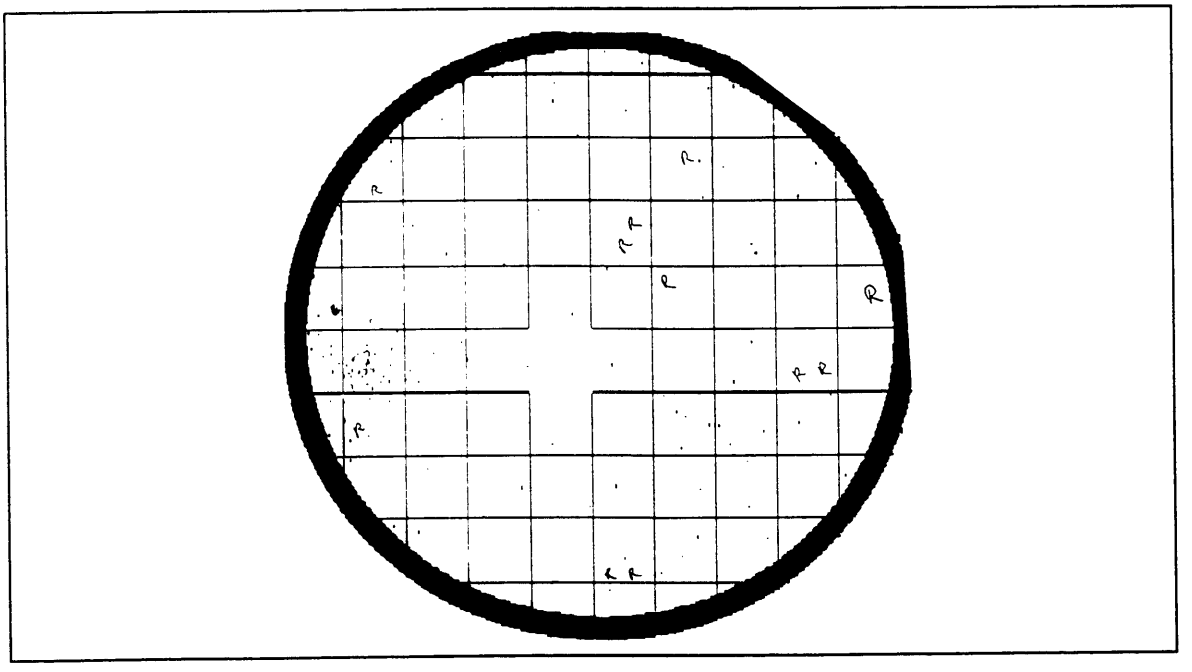

Figure 4.5 M1 particle signature.

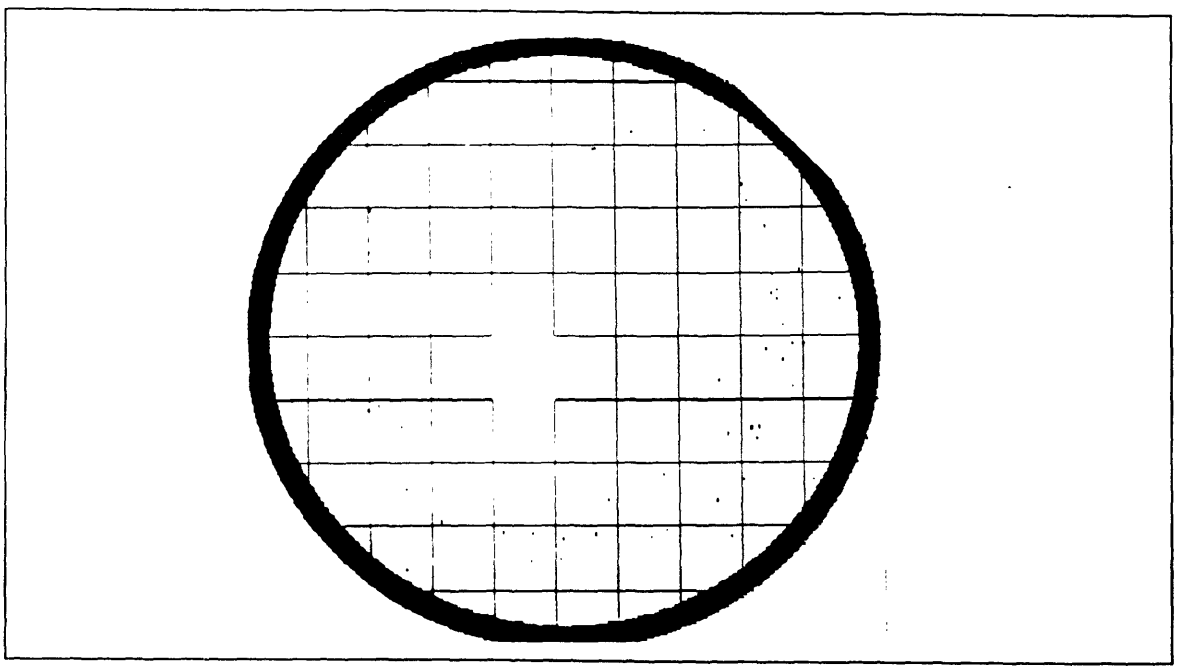

Figure 4.6 Tungsten 'cheerio' particle signature.

Chapter 5
Tungsten Particle Source Determination

5.1 Introduction

Chapter 3 presented the development of a new monitor tool to capture defects and chapter 4 correlated the optical defects to electrical defects. But what causes these defects to exist? In response to this a list of possible sources of particulates within the tungsten LPCVD system was brainstormed. Defect sources could be but were not confined to this list: 1). Gas phase particle generation, 2.) Vacuum pump down condensation particles, 3.) Backside etch (BSE) particles, 4.) Asymmetric hardware particle sources 5.) Fall-on particles (from the chamber components) and 6.) Deposition time dependent particles.

5.2 Gas Phase Particle Generation

For silane reduced tungsten hexafluoride, the literature shows gas phase particle generation occurs below a critical WF_6/SiH_4 gas flow ratio of 1 [McInerney and Mountsier, 1992]. In this regime the gases react before they can get to the surface causing high particle levels. Our LPCVD reactor operates at a flow ratio of 2 which is

considerably higher than the gas phase nucleation threshold. Increasing this number further only wastes expensive WF_6 and increases substrate attack.

5.3 Condensation Induced Particles

Pumping a chamber down above a critical rate will lead to water vapor expansion and subsequent condensation. The condensed matter then evaporates leaving a H_2SO_4 residue [Yan Ye, Liu and Pui, 1993]. Review of a Sematech Technology Transfer document on the manufacturability of our LPCVD system shows that the pump rates have been optimized and the H_20 and O_2 levels are at minimal levels.

5.4 Backside Etch Particles

5.4.1 Experimental

Particle levels have been shown to increase with chamber pressure and to a lesser degree with increased RF power [Durham, Petrucci and Steinbruchel, 1990]. Since the chamber pressure and RF power are established settings in the process, an experiment was set up to determine the particle contribution of the NF_3 plasma backside etch (BSE) process. In this experiment nine wafers were processed with BSE and nine wafers without BSE on the same chamber.

5.4.2 Results and Discussion

Appendix A contains the particle data and the statistical comparison of the BSE and no BSE conditions. The backside etch particle delta is 25% greater than the no BSE condition. This seems quite substantial; however, the standard deviation is as large as the mean delta value. Therefore, based on 95% confidence levels there is no difference

between the BSE and no BSE particle levels. Given that the measured standard deviation for the nine samples is approximately the same as the 'real' value, it would require over 400 wafers in order to prove a difference between BSE and no BSE particle levels. Hence the BSE step in the tungsten process does not appear to be a statistical significant, direct particle contributor.

5.5 Asymmetric Hardware Particle Sources

The tungsten deposition chamber does not have a symmetric design (section 2.4.1). For example the pump port in the process chamber is not symmetrically located underneath the wafer, rather to one side of the wafer. The susceptor blade and the wafer lift hoop are additional hardware parts which are located in asymmetric, unique positions within the process chamber. A possible technique of identifying these hardware items as particle sources is to analyze particle maps in order to determine whether certain areas of the wafer consistently capture more particles.

5.5.1 Experimental

Reviewed blanket tungsten particle maps in order to identify possible trends or particle signatures. Chose five wafers from each of chambers A, B, C and D (20 total wafers). The added particles were determined by comparing the pre and post deposition maps then tallying the particles according to several different schemes:

1.) Particles in a small center square 2 cm x 2 cm

2.) Particles in a larger center square 4 cm x 4 cm

3.) Particles binned into one of the four quadrants

5.5.2 Results and Discussion

The percentage of particles contained in these areas is then compared to the percentage of the total area represented. Given a random distribution of particles across the wafer, these two numbers should be equal. If certain areas of the wafer have a greater percentage of defects this could indicate particle source generation from an asymmetric hardware part. Table 5.1 contains the results for the three particle bin strategies.

Table 5.1 Particle Mapping Area Percentages

Area Represented	Defect Percentage	Area Percentage	Defect/Area Ratio
Center 2cm^2	4.6	5.1	0.90
Center 4cm^2	19.1	20.3	0.94
Quadrant I	25.0	25.0	1.00
Quadrant II	24.0	25.0	0.96
Quadrant III	25.7	25.0	1.03
Quadrant IV	25.3	25.0	1.01

The average percentage of defects in the center 2 cm^2 and 4 cm^2 of the wafer is within 10 percent of the surface area percentage. Therefore, there does not appear to be a significantly lesser number of particles near the center of the wafer compared to the rest of the wafer. The average percentage of defects in any quadrant (I, II, III, IV) of the wafer is within 5% of the surface area percentage. Hence, the presence of asymmetric hardware elements does not yield characteristic particle signatures for baseline particle levels.

5.6 Particle Flow Mechanics

Silane and WF_6 are very volatile gases which may react with chamber parts causing hardware degradation and particle generation [Hogle and Brown, 1990], [Hogle and Skow, 1992]. For example, the reactive gases flow through the blocker plate and showerhead before impinging upon the wafer. Such gas flow may dislodge particles from the hardware elements which then deposit on the wafer. The growing field of aerosol technology has developed may models and theories for particle transport. Insight on particle flow characteristics can be gained by examining Stokes Law relating particle flow characteristics.

$$F = \frac{6\pi\mu a V}{C} \qquad (5.1)$$

F = drag force on the particle

a = particle radius

μ = gas viscosity

V = particle velocity relative to the gas

C = Stokes-Cunningham slip correction factor

λ = mean free path of gas molecules

ρ = density of gas

Equation 5.1 is valid for Reynolds number $(2Va\rho/\mu) < 0.1$. For small aerosol particles and large Knudsen numbers $(\lambda/a) > 0.01$, Stokes law must be corrected to account for the effects of gas slip (C).

From this research, several process modification have been identified which could improve defect levels.

1.) Increasing deposition pressure. Greater pressures increase the drag forces experienced by particles dislodged from the showerhead. Increased drag forces will enable the particles to follow the gas streamlines and be purged from the system.

2.) Use a more porous shower head plate. For a given gas pressure entering the shower head plate, the gas accelerates as it passes through the showerhead. In essence the showerhead plate is acting like an impactor giving particles greater inertia to break the streamlines and deposit on top of the wafer.

Unfortunately, changing process parameters such as the deposition pressure or equipment modifications such as a more porous showerhead can affect other important properties such as film growth rate, uniformity and resistivity. By increasing the porosity of the plate particle impaction can be reduced, though at the cost of increasing the boundary layer above the wafer. Larger boundary layers reduce the step coverage of the deposited tungsten film causing other process marginalities [Kleijn, 1993]. In order to adopt particle reducing process changes, all other aspects of the film must be studied in order to maintain the integrity of resulting film as well as assure process synergy with preceding and following steps in the process flow.

5.7 Deposition Time Dependent Particles

5.7.1 Experimental

Tungsten films ranging from several hundred angstroms to the production thickness film of greater than 0.5 microns were deposited in the CVD reactor. All wafers were scanned for particles prior to deposition using the blanket film detector. The wafers

were then scanned after deposition and the added particles was taken as the difference between the pre-deposition and post-deposition particle counts.

5.7.2 Results and Discussion

Figure 5.1 shows the normalized particles added versus normalized film thickness. Particles levels do not increase with film thickness, rather defect levels appear to be independent of film thickness. Microscopic review work performed on these different thickness films showed that in general the deposition process does not accentuate particle size, rather the film smoothes out the contours of particles (except for organic particles which poison the area surrounding the particle leaving a 'bulls-eye' where no film is present). The existing particles do not appear to induce preferential heterogeneous nucleation nor do the particles appear to affect the film growth rate.

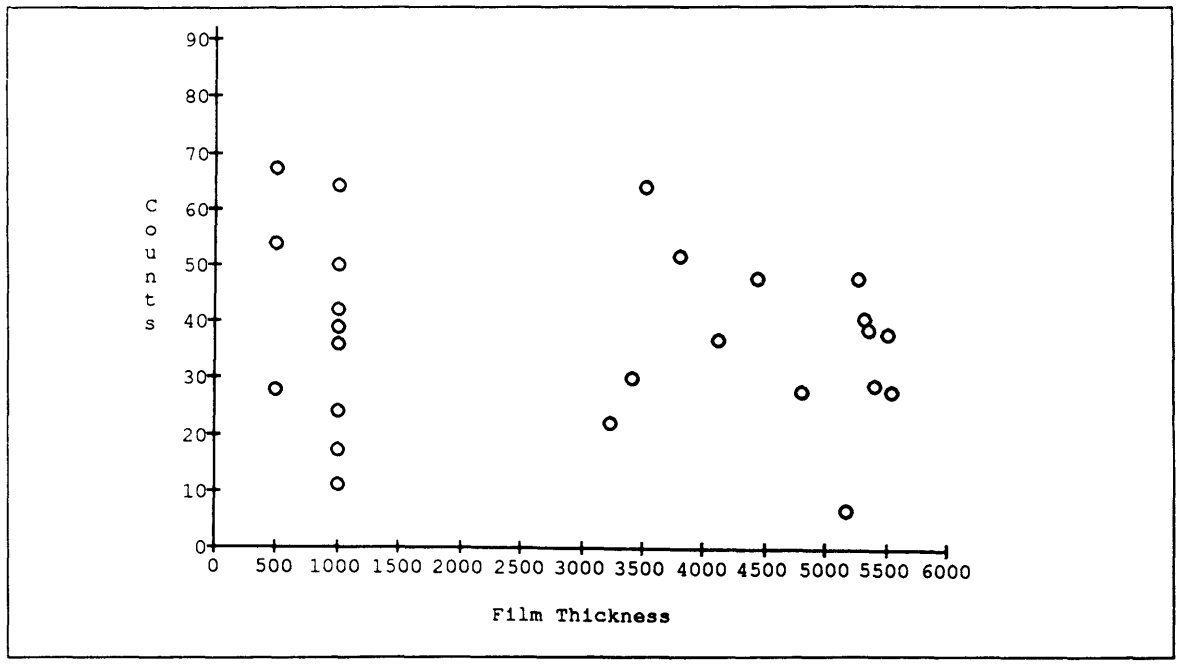

Figure 5.1 Normalized particles vs. normalized film thickness

5.8 Conclusion

Chapter 3 investigated some of the out of control excursion mode particle signatures, for example the cheerio defect pattern. However, investigation of under control particle levels has shown that baseline particle levels do not have characteristic particle signatures. Various experiments which measured the particle levels and locations under a variety of conditions were not able to confirm the presence of major particle sources such as the backside etch step or asymmetric hardware elements. In order to further characterize particle sources, elemental characterization must be performed on the defects in order to identify the particulate generating source.

Chapter 6
Particle Detection and Characterization Methodology for Blanket Films

6.1 Introduction

With sub-micron device geometries there is an increasingly greater emphasis on detecting and eliminating defects on deposited films. We present a methodology that can be used to improve the detection and characterization of defects on blanket films. By changing certain process parameters and consequently film properties, we can increase the sensitivity of conventional laser-based particle detectors. The first step is to identify the film properties which affect particle detection sensitivity. The next step is to determine the optimal film characteristics for defect detection as well as Energy Dispersive X-ray (EDX) analysis. Subsequently, particles captured in the film can be elementally analyzed in order to determine the chamber hardware particle source.

6.2 Experimental

The experimental goal was to vary the deposition times and nitrogen flow rate in order to identify the effects on surface roughness, reflectivity and resistivity. Table 6.1 contains the thickness, surface roughness, resistivity and normalized reflectivity for

variable deposition time, constant nitrogen flow rate conditions. Table 6.2 contains the normalized thickness, surface roughness, resistivity and normalized reflectivity values for the constant deposition time, variable N_2 flow rate conditions. Atomic Force Microscopy (AFM) was used to determine the Root Mean Square (RMS) surface roughness, an optical film probe measured the reflectivity and an electrical four point probe measured the sheet resistance. Reflectivity was normalized to polished bare silicon. Thickness was determined from a W/Si count-RBS standards calibration curve using X-ray Fluorescence (XRF). Resistivity was determined from the relationship between sheet resistance and thickness (resistivity equals thickness times sheet resistance).

Table 6.1 Thickness, Roughness, Resistivity and Reflectivity versus Deposition Time.

Normalized Deposition Time	Thickness (nm)	Roughness (nm)	Resistivity (μΩ-cm)	Normalized Reflectivity
0	0	1.3	-	23.0
0.14	75	2.0	-	175.8
0.67	380	15.0	12.35	62.0
0.71	480	-	11.94	55.1
0.76	530	19.7	11.72	52.6
0.86	610	-	11.37	47.2
0.90	650	23.5	11.12	45.5
0.95	690	-	10.99	43.9
1.00	735	25.9	10.94	42.5

Table 6.2 Thickness, Roughness, Resistivity and Reflectivity versus N_2 Flow Rate

Normalized N_2 Flow Rate	Normalized Thickness	Roughness (Angstroms)	Resistivity (μΩ-cm)	Normalized Reflectivity
0	0.97	25.9	11.15	52.3
1	1.03	-	11.31	65.2
1	1.02	21.9	11.32	65.7
2	1.03	-	11.64	69.5
2	1.01	-	11.65	69.8
3	1.00	19.7	11.72	75.3
3	0.98	-	11.79	76.4

6.3 Discussion

6.3.1 Defect Detection

Manufacturers of Integrated Circuits widely employ laser wafer scanners which rely upon scattered light for the detection of surface contamination. In addition to particles, however, light is also scattered by voids and grain boundaries which contribute to the surface roughness of a film. As discussed in section 2.3.3, vector diffraction theories can relate the total integrated scatter (TIS) to the surface roughness (σ) and the incident wavelength (λ).

$$TIS \approx (4\pi\sigma / \lambda)^2 \qquad (6.1)$$

Since it is necessary for the particles to be seen above the background scatter of the substrate, conditions which produce minimal background scatter and high particle

scatter optimize the detection process. According to equation 6.1, scatter is positively related to RMS surface roughness and inversely related to wavelength. Though the wavelength for our laser-based contamination analyzer is set at 488nm, the surface roughness of a film may be modified by changing certain process parameters. Figure 6.1 shows the strong positive correlation between surface roughness and film thickness for the tungsten films. Figure 6.2 shows the strong negative correlation between reflectivity, resistivity and film thickness. Appendix B contains the SEM micrographs depicting the surface morphology of the 380nm, 530nm and 735nm tungsten films. The thicker films appear rougher with slightly larger grains, however due to the complex surface morphology it was very difficult to quantify differences in grain size between the films.

Surface roughness, reflectivity and resistivity are strongly related to nitrogen flow rate. Figure 6.3 shows the positive relation between nitrogen flow rate and reflectivity and resistivity. As nitrogen flow rates increase there are diminishing increases in reflectivity as well as increasing margins in resistivity. The grains appear similar for the various process conditions though the complex surface morphology made for difficult grain size comparison. The increase in resistivity with nitrogen has also been identified for other films. Hartsough and Denison, [1979] found the resistivity of aluminum-silicon films to be positively correlated to nitrogen partial pressure. Hence, larger nitrogen flow rates have the benefit of increasing reflectivity though at the cost of increased resistivity.

The impact of this work as far as defect detection is concerned was that we were able to identify the film properties which control the light scattering behavior for tungsten films. Thinner films have less surface roughness and greater reflectivity corresponding to greater particle detection capability. To verify this, mono-disperse latex spheres were deposited on different thickness tungsten films. Latex spheres as large as five microns

could not be detected on 530nm tungsten films; however 1.0μm spheres were easily detected on 100nm tungsten films.

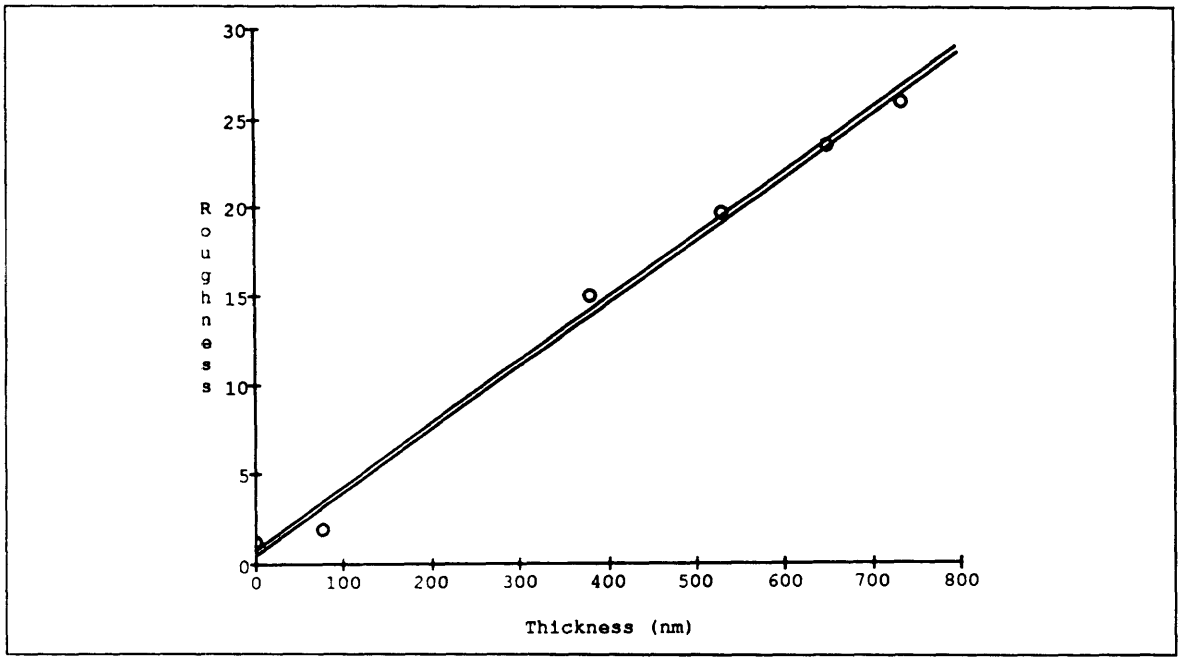

Figure 6.1 Surface roughness versus film thickness

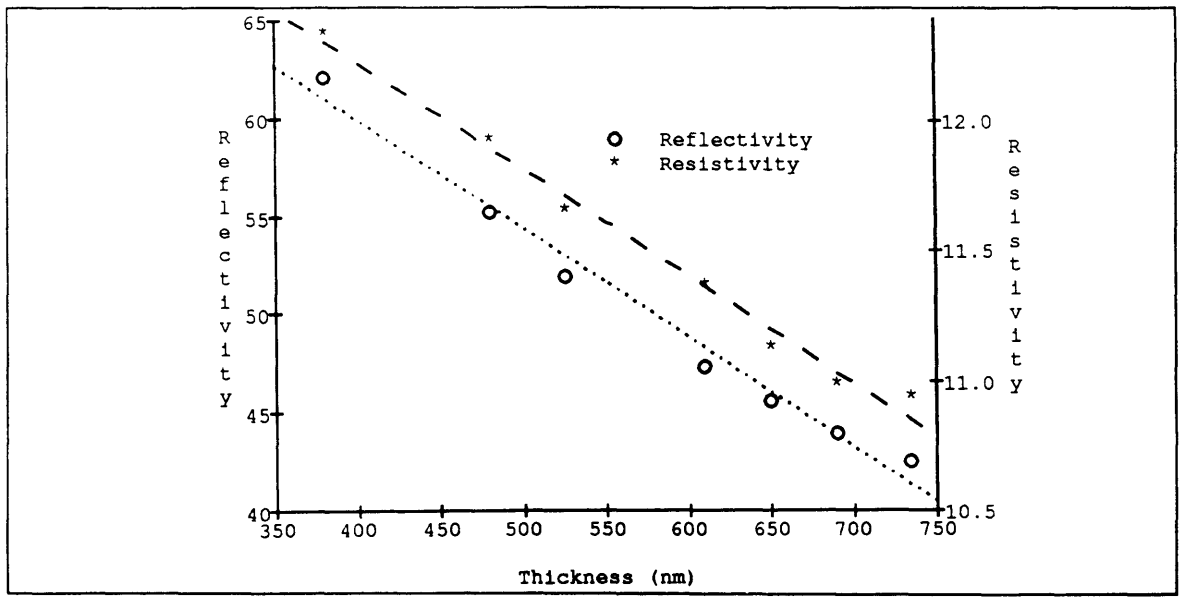

Figure 6.2 Resistivity and reflectivity versus film thickness.

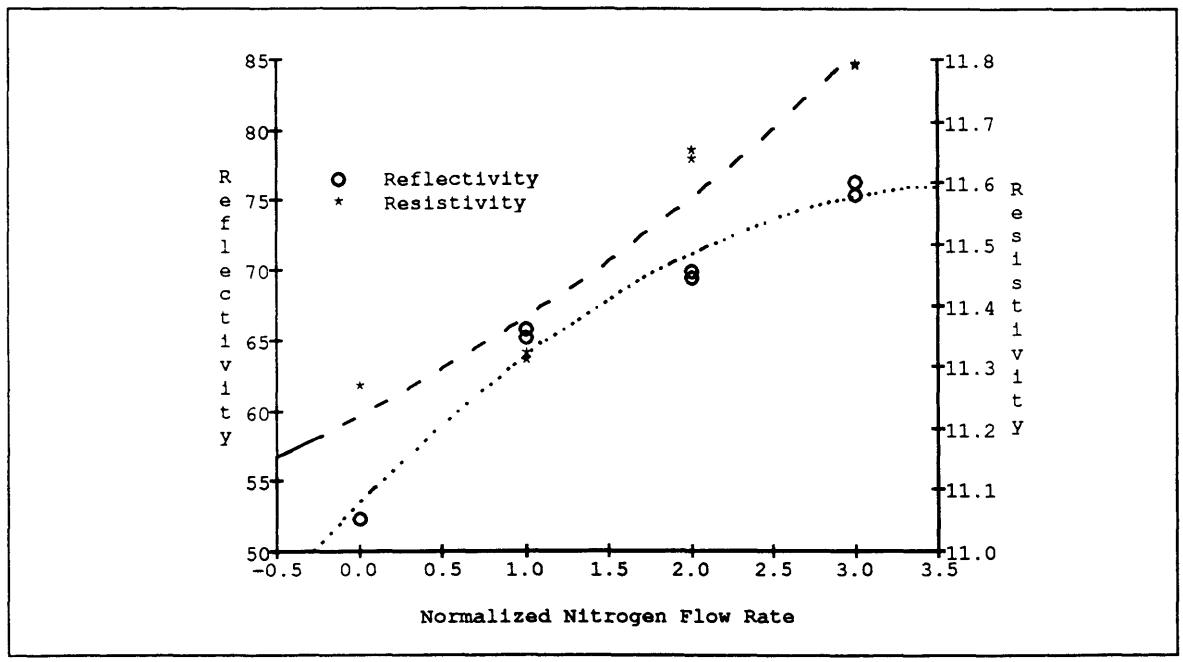

Figure 6.3 Normalized nitrogen flow rate versus reflectivity and resistivity.

6.3.2 Energy Dispersive X-Ray Capability

In addition to laser wafer scanning criteria, the EDX capability must also be considered when choosing the optimal monitor film. In many respects, EDX analysis of particles is similar to light scattering analysis of particles. In the case of EDX analysis, the elemental of the defect must be distinguished from the background elements, whereas in defect detection the light scatter from a particle must be distinguished from the background scatter. In order to enhance the elemental characterization of an EDX system, both the electron penetration depth and the interaction volume must be considered. For an EDX system, the formula for electron penetration depth is

$$d = \frac{4120}{\rho} E^{(1.265 - 0.0954 \ln E)} \qquad (6.2)$$

where d is the penetration depth in microns, E is the primary electron energy in MeV and ρ is the material density in g/cm^3.

Using typical density values for CVD tungsten film, the calculated electron penetration depth is roughly 200nm for a 15KeV electron beam and 1000nm for a 35KeV beam. A more energetic electron beam increases the penetration depth, however this also increases the interaction volume causing greater substrate and background signals. Monte Carlo simulations of the electron path, representative interaction volumes can be identified. Figure 6.4 compares the simulated interaction volume for 15KeV and 35KeV electron beams penetrating tungsten. When analyzing defects within a 1000nm film, at least a 35KeV beam must be used to characterize particles buried deep within the film. For sub-micron particles, however, the interaction volume of a 35KeV beam can be orders of magnitude larger than the particle. On the other hand, if a 100nm film was analyzed, a

15KeV beam would have sufficient penetration depth to characterize particles added during the early stages of film growth. Therefore, thinner films allow lower energy, smaller interaction volume electron beams to be used in order to reduce the background noise and improve the elemental characterization of defect.

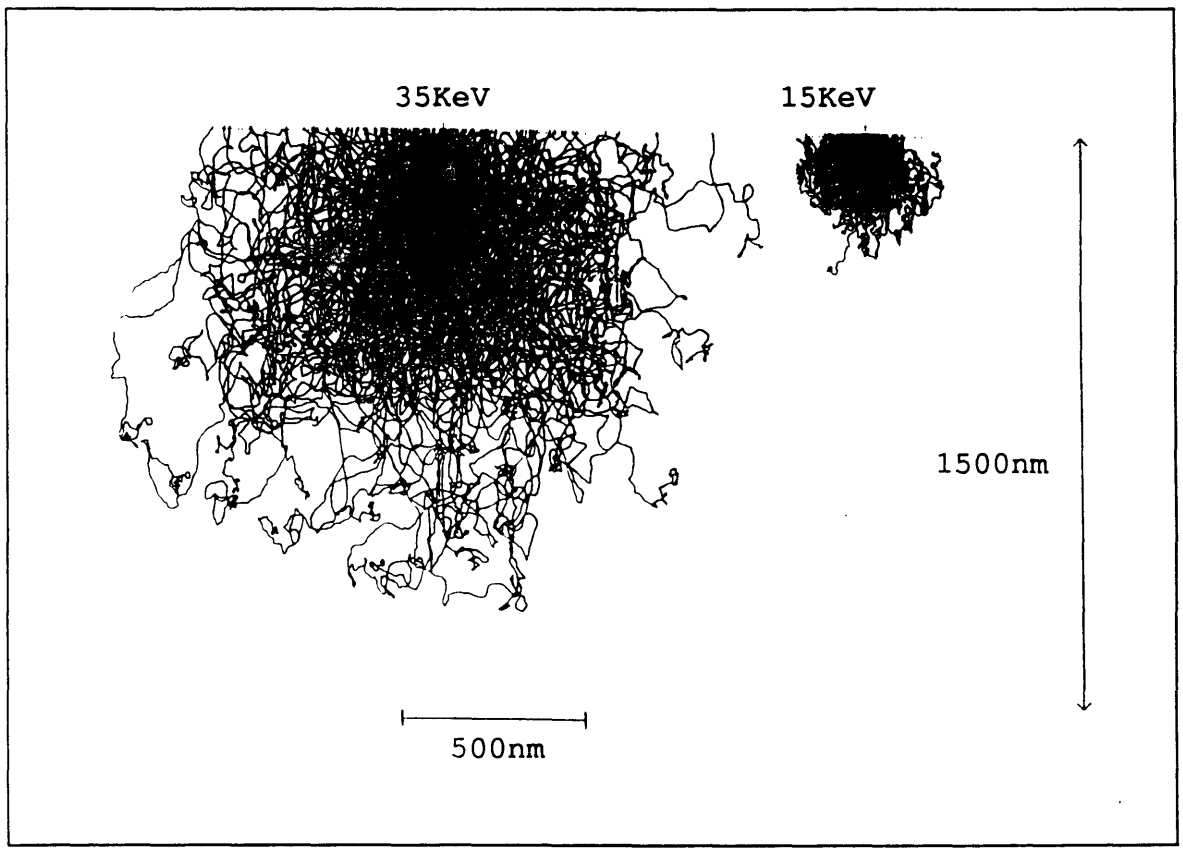

Figure 6.4 Comparison of Monte Carlo simulations of electron interaction volumes for 15KeV and 35KeV beams penetrating tungsten.

Another consideration for EDX capability is the substrate material. For tungsten films that are deposited on a titanium nitride/borophosphosilicate glass/silicon substrate it is possible for the EDX tool to detect the elements not only from the defect, but also from

the underlying layers. In this case, the titanium, nitrogen, boron, phosphorous, silicon and oxygen from the background signal may confound the particle's unique elemental signature. By depositing the tungsten film directly on silicon the number of confounding background elements would be reduced. Such a technique was attempted but the resulting film roughness was very high. Hence the contamination analyzer could only identify particles sized larger than 1.5 microns. Apparently, the tungsten hexafluoride etches the silicon substrate as well as reacting with the silane. This reaction roughens up the surface resulting in a greater background scatter and reduced particle resolution. Although the background signal is more complex, titanium nitride/inter layer dielectric was chosen as the substrate film.

6.3.3 Particle Levels

In addition to allowing more sensitive particle detection, thinner films also improve the elemental characterization of particles. However, too thin of a film may not adequately represent the process sequence as that of a product level film. More specifically, the particle levels for a thinner film may not reflect the true defect density of a production thickness film. To this extent, particle levels were tracked on different thickness tungsten films and then compared to the particle levels experienced by our production level film. Figure 5.1 shows that blanket film defect levels are not correlated to film thickness.

6.3.4 The Optimal Film

Given the constraints on particle detection, characterization and overall particle levels, a 75nm of tungsten was chosen as the optimal film thickness. By depositing such a

film on a titanium nitride adhesion layer, full electron penetration was achievable at 10KeV and a minimum particle detection threshold was set at 0.3 microns.

6.3.5 Particle Characterization Flow Sequence

The flow sequence in characterizing particles on blanket films is:

1.) Using a laser based contamination analyzer, perform a pre-deposition scan of the wafer and obtain a particle map. A pre-deposition scan determines the pre-existing particle levels and locations.

2.) Deposit 750nm tungsten film.

3.) Perform a post-deposition scan and obtain a particle map. Visually compare pre and post deposition maps in order to identify the location of added particles. Software tools exist which may also be used to distinguish the added defects

4.) Using a mechanical or laser scribe, make characteristic lines and dots at opposites sides of the wafer. Since the substrate is not patterned, deskew points must be added to the film surface in order to cross-reference the location of the defect.

5.) Microscopically review particles using software that drives the microscope stage to the particle coordinate as identified by the defect map.

6.) Perform SEM/EDX analysis at 5 and 15KeV on optically identified particles.

7.) Match elemental composition of defect to known composition of chamber hardware components. The elemental composition of the hardware can be determined by performing EDX analysis on surface samples taken from the various chamber parts. Indium foil sampling of exposed hardware sources has proven to be a useful method at fingerprinting chamber parts.

6.4 Conclusion

For conventional laser-based particle counters, defect detection capabilities are dependent on parameters such as the wavelength of the incident light and the surface roughness of the film. For EDX systems, defect characterization is dependent on film properties such as the density and thickness of the film. Though the incident wavelength and the film density in most cases are constant, the surface roughness and thickness of a film can be modified. In our case for tungsten, by reducing the film thickness we were able to detect and characterize much smaller defects added by our system.

Chapter 7
Particle Characterization

7.1 Introduction

Chapter 5 presented several experiments used to identify particulate sources. However, in addition to performing experiments, particles can also be characterized by their size and elemental composition using laser-based particle detectors combined with Scanning Electron Microscopy (SEM)/Energy Dispersive X-Ray (EDX) analysis. By tracking particles throughout the PM cycle, suspect chamber hardware elements may be identified by matching the elemental signature of the particle to the composition of the hardware part.

7.2 Experimental

The experimental goal was to identify the elemental composition of the defects added by the tungsten LPCVD system. Defects from chambers A, B, C and D were

optically identified and elementally analyzed at three specific stages: Immediately after a Preventative Maintenance (PM) wet clean, mid-way, and prior to the next wet clean.

Optical defects were identified by a laser-based contamination analyzer using two defect monitoring techniques.

1.) The bare wafer technique involves processing a polished silicon wafer through the tungsten process sequence without reactive gas flows. Only carrier gases flow through the chamber so no film is deposited. The minimum particle detection threshold for the bare wafer monitor is 0.2 microns.

2.) The blanket film technique involves depositing a 75nm tungsten film on a titanium nitride/inter layer dielectric/silicon wafer. The minimum particle detection threshold for the blanket film monitor is 0.3 microns.

The wafer monitoring process sequence for all four chambers, A, B, C and D was:

1.) Standard film thickness wafer processed.

2.) Bare wafer (no reactive gas flow) wafer processed.

3.) 75nm Blanket tungsten film processed.

After wafer processing, every added defect from the bare wafer and blanket film monitor was microscopically reviewed using the procedure established in section 6.3.5. Afterwards, representative defects from each stage of the chamber clean cycle were submitted for SEM/EDX analysis.

7.3 Results and Discussion

Of the two monitoring techniques employed, the bare wafer monitor produced more defects than the blanket film monitor. The greater number of defects detected by the bare wafer monitor can be attributed to its smaller particle detection threshold compared to the blanket film monitor (0.2mm vs 0.3mm). The defects detected by both monitors; however, were both optically and elementally similar.

7.3.1 Defect Histograms

Figure 7.1 compares the particle detector sizing to the measured maximum particle dimension for the bare wafer monitor. The tool sizing was performed automatically by matching the scattering cross section of the particle to a scattering cross section/latex sphere calibration curve. The measured particle sizing was taken using SEM and optical photos. Figure 7.2 compares the particle detector sizing to the measured maximum particle dimension for the blanket film monitor. The histograms for both the bare wafer and blanket film defects have similar distribution with 75% of all defects having a maximum dimension less than 1 micron. For both the bare wafer and blanket film monitors, the particle detector consistently under-sized the particles. Part of this discrepancy is because the sizing measurement was taken from the maximum particle dimension; however, even for more spherical particles analyzed, the particle detector consistently under-sized the particles.

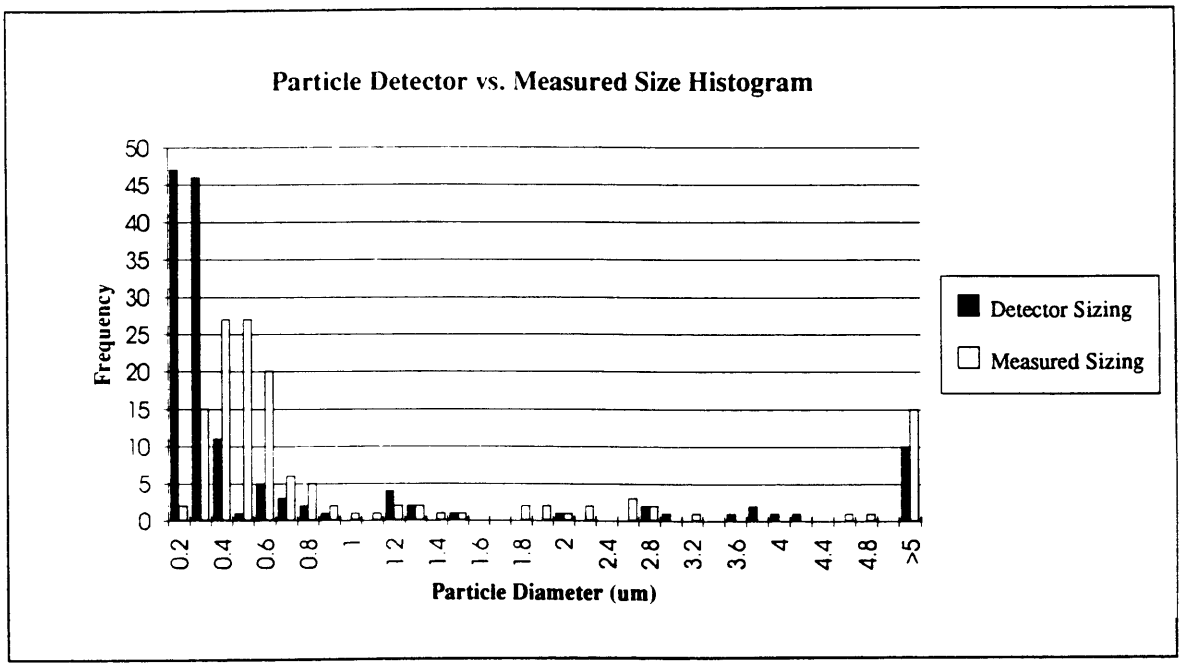

Figure 7.1 Bare Wafer Particle Sizing Histogram

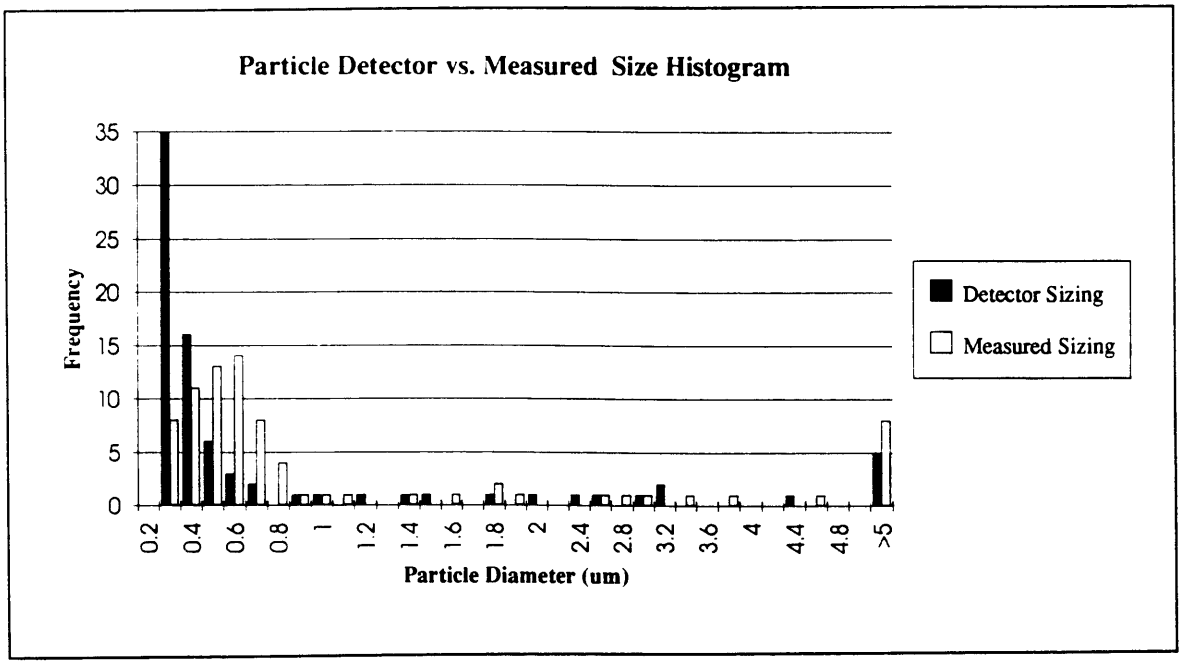

Figure 7.2 Blanket Film Particle Sizing Histogram

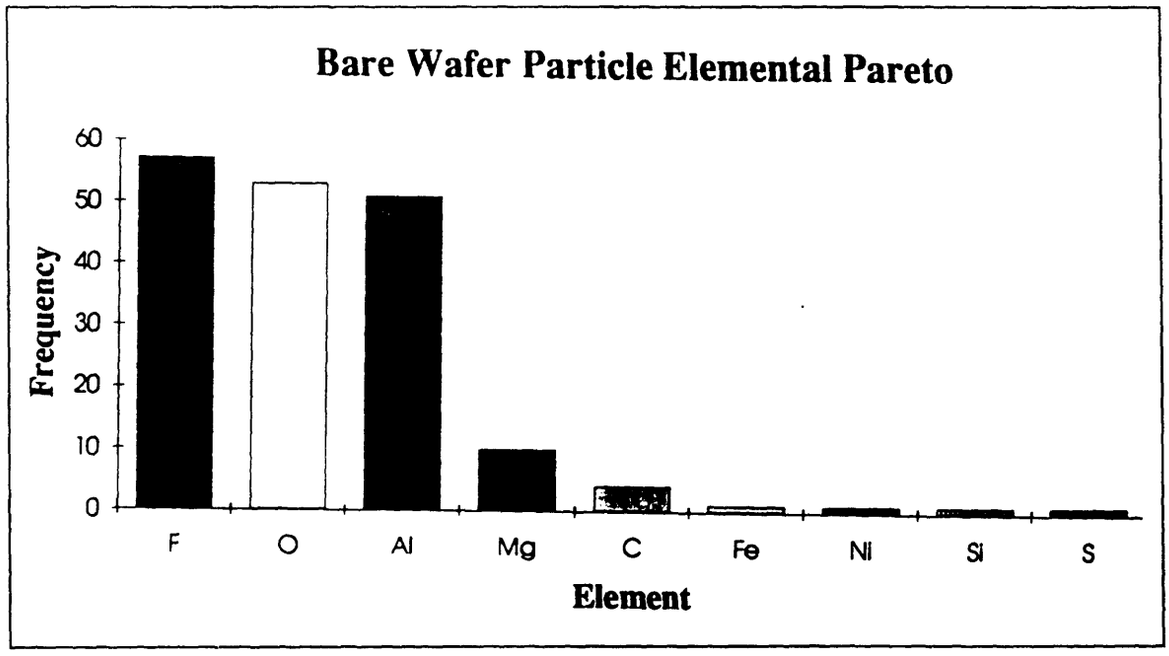

Figure 7.3 Bare Wafer Particle Elemental Pareto

7.3.2 EDX Characterization

Figure 7.3 shows the elemental breakdown for the particles analyzed on bare wafers. The largest elemental categories are F, O and Al. Combining the results from optical and scanning electron microscopy with EDX analysis, we have characterized our largest defect category as aluminum fluoride particles having a median size distribution of 0.5 microns. One of the main sources of these defects has been identified as the aluminum showerhead which is degraded by the fluorine-containing reactive gases during deposition and chamber cleans. The second largest defect category has been classified as greater than one micron flakes which contain aluminum, magnesium and fluorine. These defects have been traced to the susceptor which contains small amounts of magnesium.

7.3.3 PM Cycle Particle Trends

In one of the two instances where particles were tracked through the PM cleaning cycle, there was an upward trend in >1.0 micron flakes. EDX analysis showed these flakes to contain aluminum, fluorine, oxygen or aluminum, fluorine and magnesium. Further investigation showed that the susceptors from the chambers had processed from two to four thousand wafers. These defects have been traced to the aluminum susceptor which contains small amounts of magnesium.

7.4 Conclusion

Comparison of the defects detected by the blanket and bare wafer monitors revealed that the reactive gas flow did not appear to generate any additional particles compared to the no reactive flow monitor. The largest particle category has been identified as 0.3 to 0.8μm aluminum fluoride flakes which most likely originate from the showerhead. Other particle categories were much smaller and not consistently present on the monitor wafers. In one of two instances there was an increasing trend in >1.0μm flakes; however, there were still four times as many of the smaller bin, aluminum fluoride defects.

The presence of fluorine containing gases during deposition (WF_6) and inter-wafer chamber cleaning (NF_3) appears to degrade the chamber causing different fluoride particles to be generated. Further work needs to address reducing the degrading effects of these gases, for example, by reducing the chamber clean times.

Chapter 8
Summary and Suggested Future Work

8.1 Tungsten Particle Monitoring

Presently two wafers are required per chamber for particle monitoring, the bare wafer monitor with a particle detection threshold of 0.2 microns and the blanket film monitor with a detection threshold of 0.4 microns. The bare wafer monitor is used since it captures smaller defects than the blanket film monitor, while the blanket film method can also be used to monitor film properties such as reflectivity, resistivity and uniformity. A preferred technique would be to monitor defects down to 0.2 microns on a blanket wafer. Hence, the bare wafer monitor would be eliminated saving thousands of dollars in wafer costs as well over a year in addition to reducing the time required to perform monitors.

The equipment supplier for our laser-based contamination analyzers has recently introduced a new detector that has better than 0.2 micron particle resolution for most rough surfaces. Such a tool would capture the smaller bin defects not presently detected by the blanket film particle tool in addition to the cheerio and Bulls-Eye defects. Further

work needs to be performed to verify if the new tool can detect all presently identified defect types in addition to the cost-benefit analysis associated with such an equipment change.

8.2 Particle Characterization

Gases containing fluorine, such as WF_6 and NF_3, are known to react with plastic and metallic materials [Hogle and Skow, 1992]. The presence of fluorine in most of the elementally analyzed particles indicates that the reaction of these gases with the hardware components is the main source of particulates. Further work designed to reduce hardware particles can be concentrated in two directions, either to use materials which are less reactive with fluorine containing gases or to reduce the equipment exposure time to such gases.

Material changes such as plating hardware parts with less reactive metals could be a valid solution at reducing particulates and improving hardware lifetimes. However, due to issues such as cost-effectiveness, durability, adhesion and differences in thermal expansion, the material solutions investigated thus far have been unsuccessful.

A second approach is to reduce the time that the chamber elements are exposed to the reactive gases. Although the deposition time has been determined based on process integration issues, several other steps within the process flow may be reduced. For example, the inter-wafer chamber cleans times have not been optimized. Our present clean times remove all of the tungsten from the chamber parts, however the fluorine-containing gases also attack the hardware. By installing a Residual Gas Analyzer (RGA) within the chamber the outgassed molecules may be tracked. Therefore, the removal of

tungsten containing molecules can be properly endpointed reducing further hardware degradation yet effectively removing all the deposited tungsten.

Longer term approaches such as eliminating the backside etch may also improve particle performance as well as increase hardware lifetimes. Presently, LPCVD tungsten tools which prevent backside deposition exist and are being used in other manufacturing environments. However, the cost of changing deposition systems must be weighed against the benefits of lower particles and reduced hardware degradation.

Appendix A

Particle Data and Statistical Comparison of the BSE and no BSE Data

Normalized BSE versus No BSE Particle Data

	With BSE	No BSE
1	1.000000	0.051282
2	-0.102564	0.346154
3	0.282051	-0.243590
4	0.589744	0.102564
5	0.025641	0.756410
6	0.858974	0.692308
7	0.500000	0.461538
8	0.282051	0.820513
9	0.487179	0.179487

Comparison of 2 samples

Null Hyp: Mean of population 1 = Mean of population 2
Alt Hyp: Mean of population 1 <> Mean of population 2

	Sample 1		Sample 2
Mean	0.4359		0.3519
Standard Deviation	0.3594		0.3619
# of points	9.0000		9.0000
Diff of Means		0.084000	
SE of Diff of Means		0.170000	
95 percent Confidence In	-0.2764	< Diff <	0.4445
t statistic		0.494300	
p-value		0.627788	

Because the p-value of 0.6278 is greater than 0.05, the null hypothesis cannot be rejected at the 5 percent level.

Appendix B

SEM Micrographs of Different Thickness Tungsten Films

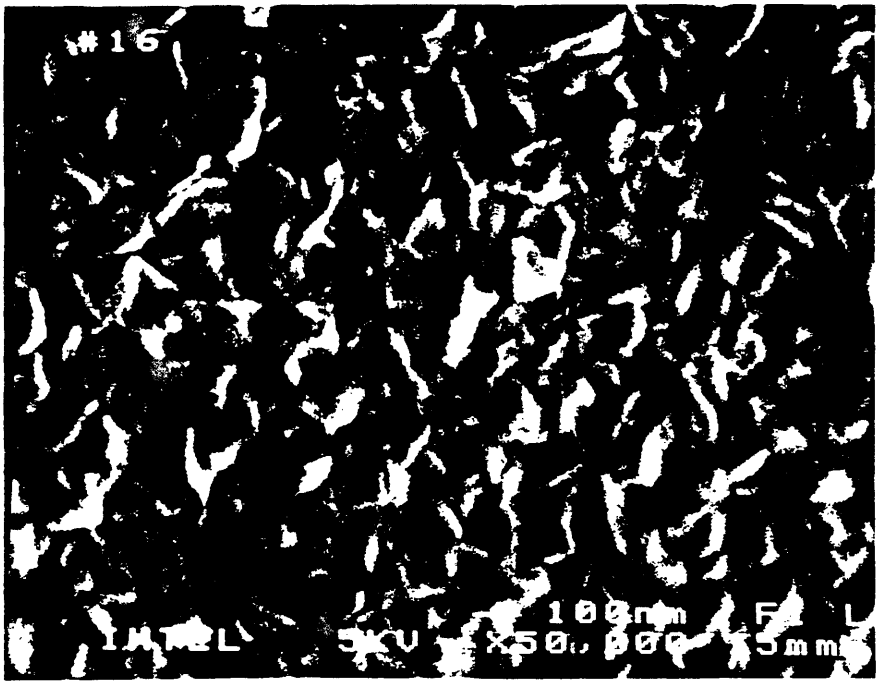

380 nm tungsten film.

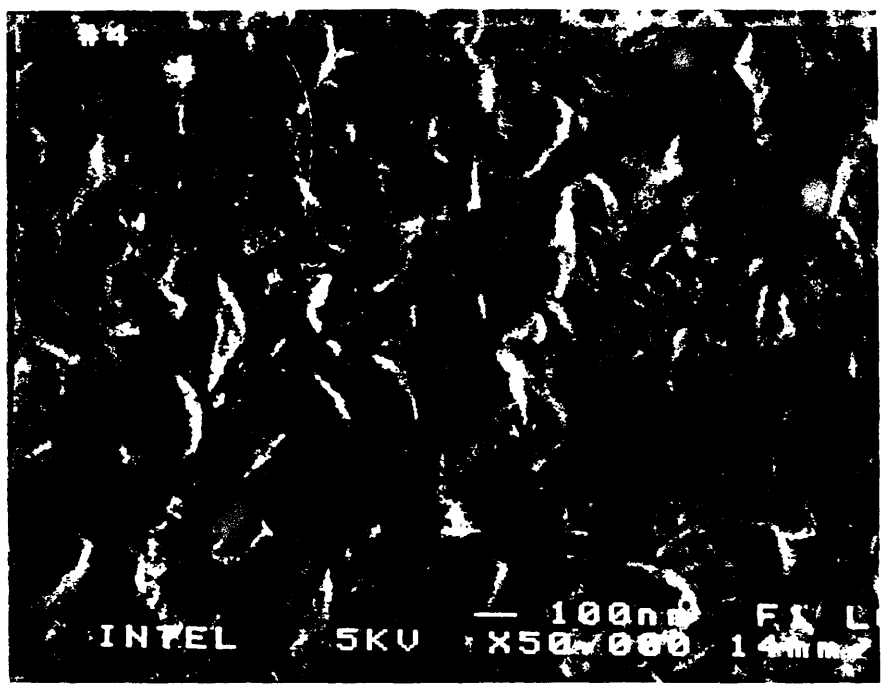

530 nm tungsten film.

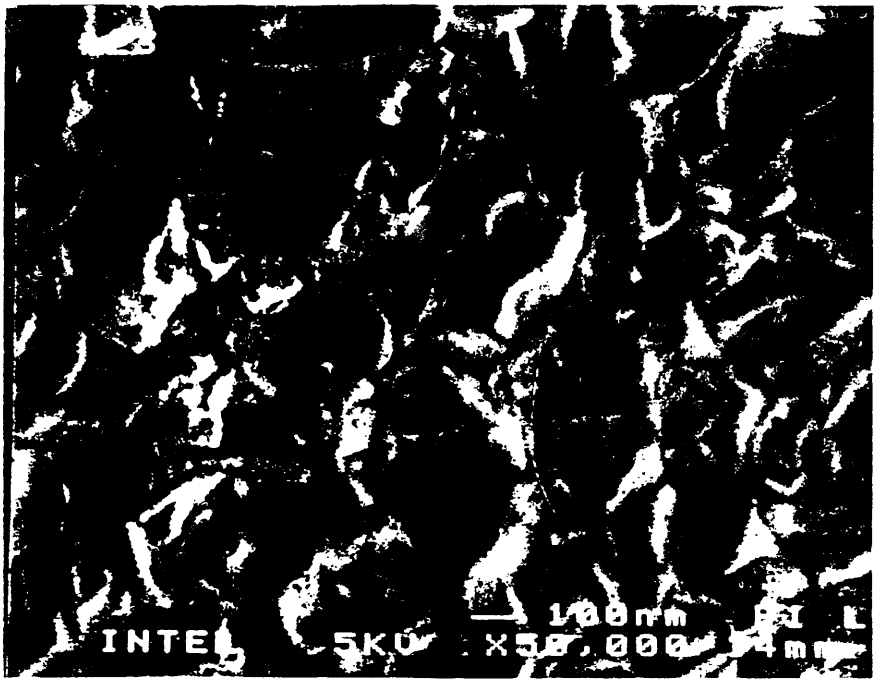

750 nm tungsten Film

References

Bawolek, E.J., and Hirleman, E.D. "Surface Roughness Effects on Light Scattered by Submicron Particles on Surfaces." SRC Publications, Arizona State University, March 1991.

Bawolek, E.J., Mohr, J.B., Hirleman, E.D., and Majumdar, A. "Light Scatter from Polysilicon and Aluminum Surfaces and Comparison with Surface Roughness Statistics by AFM." SRC Publications, Arizona State University, January, 1993.

Cale, T.S., Gandy, T.H., and Raupp, G.B. "A Fundamental Model For Transport and Deposition of Blanket Tungsten Films." Tungsten and Other Advanced Metals for ULSI Applications VI, MRS Publishers, Pittsburgh, PA, 1991.

Chatterjee and C.M. McConica, Journal of the Electrochemical Society, 137, 328, 1990.

Church, E.L., and Zavada, J.M. "Relationship Between Surface Scattering and Microtopographic Features." Journal of Optical Engineering, 18, 1979.

Durham, J.A., Petrucci, J.L., and Steinbruchel, C. "Observing Effects of Source Material, Plasma Chemistry, Process Parameters, and RF Frequency on Plasma Generated Particles." Microcontamination, 37-39, November 1990.

Elson, J.M. and Bennett. J.M. "Vector Scattering Theory." Journal of Optical Engineering, 18, 116-124,1979.

Goodman, D.W. and Rye, R.R. "Hydrogen Dissociation on Transition Metal Surfaces: The Effects of Surface Impurities." Tungsten and Other Refractory Metals for VLSI Applications, MRS Publishers, Pittsburgh, PA, 1985.

Hartsough, L.D. and Denison, D.R. "Aluminum and Aluminum Alloy Sputter Deposition for VLSI." Solid State Device Technology 22(12), 66, 1979.

Hindman, G.T. and Raupp, G.B. "Coadsorption of WF6 and H2 on Polycrystalline Tungsten: Implications for the Hydrogen Reduction Reaction." Advanced Metallization for ULSI Applications, MRS Publishers, Pittsburgh, PA, 1992.

Hinds, W.C. Aerosol Technology. New York: John Wiley and Sons, 1982.

Hogle, R.A. and Brown, P.C. "Chemical Interactions with Tungsten Hexafluoride."

Tungsten and Other Advanced Metals for ULSI Applications in 1990, MRS Publishers, Pittsburgh, PA, 1991.

Hogle, R.A. and Skow, P. "Chemical Interactions in LPCVD Tungsten Systems." Advanced Metallization for ULSI Applications:, MRS Publishers, Pittsburgh, PA, 1992.

Hsieh, J. and Joshi,R.V. "Modeling of Mass Depletion Effect on High Rate W-CVD Process." Advanced Metallization for ULSI Applications:, MRS Publishers, Pittsburgh, PA, 1992.

Hussein, M. "LPCVD Tungsten Multilayer Metallization for VLSI Systems.", University Microfilms International, Ann Arbor, MI, 1988.

Jacobson, R.D. Wilson, R.S., Al-Jumaily, G.A., McNeil, J.R., Bennett, L.M., and Mattsson, L. "Microstructure Characterization by Angle-Resolved Scatter and Comparison to Measurements Made By Other Techniques." SRC Publishers, University of New Mexico, June 1992.

Kleijn, C. "Numerical Modeling of CVD Equipment as a Tool for Process Optimization and Reactor Design.", Presentation given at Intel Corporation, Santa Clara, CA, November 3, 1993.

McInerney, E.J., Mountsier, T.W. "Gas Phase Nucleation with Silane Reduced CVD Tungsten." Advanced Metallization for ULSI Applications:, MRS Publishers, Pittsburgh, PA, 1992.

McInerney, E.J., Chin, B.L. and Broadbent, E.K. "The Rate Kinetics of High Pressure CVD Tungsten." Advanced Metallization for ULSI Applications:, MRS Publishers, Pittsburgh, PA, 1992.

McInerney, E.J., Mountsier, T.W. "The Rate Mechanisms of Silane Reduced CVD Tungsten." Advanced Metallization for ULSI Applications:, MRS Publishers, Pittsburgh, PA, 1992.

Ramesh, S., Mansour, S. "Six Sigma Specification in the Quality Journey." Statistical Methods Symposium, Sematech Technology Transfer, May 15, 1992.

Rao, G.K. Multilevel Interconnect Technology. McGraw-Hill, San Francisco, 1993,

Shewhart, W. "Statistical Method from the Viewpoint of Quality Control." Dover

Publications, Inc, New York, 1986.

Spanos, C.J., Guo, H., Miller, A., Levine-Parrill, J. "Real-Time Statistical Process Control Using Tool Data." SRC Publications, Berkeley, CA, December, 1992.

Yan Ye, B., Liu, Y.H., and Pui, D.Y. "Condensation-Induced Particle Formation During Vacuum Pumpdown." Journal of the Electrochemical Society, 1463-8,140, No. 5, 1993.

Zierath, D.J. and Ramchandar, T.K. "Rapid Analysis of Particle Defects in a Single Wafer Metal CVD System in a Manufacturing Environment." Proceedings from the 1993 VLSI Metallization Symposium, 1993.

Zook, M. "Nucleation Layer Effects on CVD Blanket Tungsten Deposition." Tungsten and Other Advanced Metals for ULSI Applications in 1990, MRS Publishers, Pittsburgh, PA, 1991.